

Transitions in the Mass-ratio and Spin Properties of Binary Black Holes in GWTC-5

Elizabeth Flanagan,^{1,*} Fabio Antonini,¹ Thomas Callister,² Debatri Chattopadhyay,³ Fani Dosopoulou,¹ Isobel Romero-Shaw,¹ and Jakob Stegmann⁴

¹*Gravity Exploration Institute, School of Physics and Astronomy, Cardiff University, 5 The Parade, Cardiff, CF24 3AA, United Kingdom*

²*Williams College, Williamstown, MA 01267, USA*

³*Center for Interdisciplinary Exploration and Research in Astrophysics (CIERA) and Department of Physics & Astronomy, Northwestern University, 1800 Sherman Ave, Evanston, IL 60201, USA*

⁴*Max Planck Institute for Astrophysics, Karl-Schwarzschild-Str. 1, 85748 Garching, Germany*

We analyze the mass-ratio and effective-spin (χ_{eff}) distributions of binary black hole mergers in the latest gravitational-wave catalog, GWTC-5, as a function of primary mass. Using hierarchical Bayesian inference with flexible Gaussian-process population models, we identify four distinct mass regions separated by sharp transitions in both mass-ratio and spin properties. Below $\sim 15 M_{\odot}$, the population strongly favors equal-mass binaries and exhibits a narrow χ_{eff} distribution peaked at positive values. In the range $18\text{--}30 M_{\odot}$, the mass-ratio distribution becomes substantially flatter, while the χ_{eff} distribution broadens, shifts to a peak consistent with zero, and shows tentative—but not statistically required—evidence for positive skewness. The region associated with the feature near $\simeq 35 M_{\odot}$ returns to a narrow χ_{eff} distribution consistent with symmetry at zero and strongly favors equal-mass binaries. Above $\simeq 45 M_{\odot}$, both the mass-ratio and χ_{eff} distributions broaden significantly. The inferred support of the spin distribution converges toward the range expected for binaries containing remnants of previous black hole mergers, making the highest-mass region fully consistent with a star cluster population of hierarchical mergers. The close correspondence between transitions in mass ratio and effective spin suggests that different primary-mass ranges trace distinct formation channels, with isolated binary or triple evolution likely dominating the lower-mass population and dynamical assembly becoming increasingly important at higher masses.

I. INTRODUCTION

The latest gravitational-wave catalogue, GWTC-5 [1, 2], has significantly expanded the sample of observed binary black hole (BBH) mergers [1, 3–7], enabling increasingly detailed studies of the underlying black hole population [7]. While early analyses focused primarily on constraining the overall mass and spin distributions, the growing number of detections has begun to reveal evidence for additional structure within the population [7–11]. In particular, several studies have suggested the presence of multiple subpopulations distinguished by their masses, spins, and mass ratios [12–21]. Features such as the excess of high-mass mergers, the existence of systems in or near the pair-instability mass gap, and correlations between spin and mass all point toward the possibility that BBHs form through multiple astrophysical channels [22–31].

Black hole spins provide a powerful diagnostic of binary formation channels [32]. The best-measured spin combination in gravitational-wave observations is the effective spin parameter [33, 34],

$$\chi_{\text{eff}} = \frac{m_1 \chi_1 \cos \theta_1 + m_2 \chi_2 \cos \theta_2}{m_1 + m_2}, \quad (1)$$

where m_1 and m_2 are the primary and secondary component black-hole masses, χ_1 and χ_2 are their dimensionless spin magnitudes, and θ_1 and θ_2 are the tilt angles

between the individual black-hole spins and the orbital angular momentum. Different formation scenarios are expected to produce distinct signatures in both effective spin and mass ratio. In isolated binary evolution, tidal interactions and binary mass transfer are generally expected to align the spins of the black holes with the orbital angular momentum [35–37], leading to preferentially positive values of χ_{eff} . These channels also tend to favor binaries with nearly equal masses due to the coupled evolution of the stellar progenitors [38–40]. By contrast, binaries assembled dynamically in dense stellar environments such as globular clusters or nuclear star clusters are expected to have nearly isotropic spin orientations, producing χ_{eff} distributions centered at zero and symmetric, extending to negative values [41–44]. Dynamical channels can additionally generate a broader range of mass ratios when hierarchical mergers contribute to the population [e.g., 43]. In such systems, merger remnants from previous generations can pair with lower-mass black holes, flattening the mass-ratio distribution and producing more asymmetric binaries together with larger black hole masses and higher spins [45–47].

Additional formation channels may also contribute to the observed BBH population. In hierarchical triple systems, Lidov–Kozai oscillations can efficiently drive binaries to merger while generating substantial spin-orbit misalignment [48–52]. These channels naturally produce χ_{eff} distributions concentrated near zero but with substantial support extending to both positive and negative values. Triple-mediated mergers are expected to yield a mass ratio distribution peaked at ~ 1 but with a signifi-

* FlanaganE1@cardiff.ac.uk

icant tail at lower values [53]. Mergers occurring within active galactic nucleus (AGN) disks provide another possible formation pathway [54–56]. Gas torques and migration traps inside the disk can promote repeated mergers and partial spin alignment, potentially producing systems with large masses, high spins, and asymmetric mass ratios [56, 57]. Finally, primordial black holes constitute a qualitatively different scenario in which BBHs form in the early Universe rather than through stellar evolution [58, 59]. Depending on the primordial clustering and merger history, these models can produce broad mass-ratio distributions and generically predict very small intrinsic spins, leading to χ_{eff} distributions sharply peaked near zero [60, 61]. However, recent models show that primordial black holes might also achieve large spins [62].

Recent analyses have found growing evidence for such correlations, and, in particular, that the effective spin distribution evolves with black hole mass [16, 25, 63–67]. Moreover, binaries with a primary mass $m_1 \gtrsim 45M_\odot$ have been shown to have a broader χ_{eff} distribution than lower-mass systems [14, 22, 26, 68–73]. This behavior is consistent with an increasing contribution from hierarchical mergers formed in dense clusters and indicates the emergence of a distinct high-mass population. Other studies have similarly argued that the observed BBH population cannot be fully described by a single smooth spin distribution [22, 74–77].

At the same time, correlations between the mass-ratio distribution, primary mass, and spins have begun to emerge in recent analyses [7, 16, 40, 70, 78]. Ref. [7] finds that the effective inspiral spin distribution is broader for unequal-mass binaries and likely broadens with increasing redshift. Measuring how the spin and mass-ratio distributions evolve jointly with primary mass may provide a direct way to identify transitions between different BBH formation channels and determine whether the observed BBH population is composed of multiple astrophysical components rather than a single smoothly evolving distribution [79, 80].

In this work, we investigate how the effective-spin and mass-ratio distributions evolve with primary black hole mass using the GWTC-5 catalogue. Our analysis combines flexible non-parametric Gaussian-process models with simpler parametric descriptions, allowing us to identify which features are robustly supported by the data and which depend on modeling assumptions. In particular, we test whether the observed population is consistent with a single smoothly evolving distribution or whether the data favor the emergence of distinct subpopulations with different spin and mass-ratio properties at different masses. The increased number of detections in GWTC-5 enables significantly tighter constraints on the possible contribution of hierarchical mergers to the high-mass BBH population and allows us to search for evidence of population transitions as a function of mass and make a stronger connection to astrophysical formation scenarios. We identify four mass regions across which the mass-ratio and spin distributions change, with transitions at approx-

imately 15, 35, and 45, M_\odot . This behavior is consistent with a scenario in which isolated binary or triple evolution dominates the lowest-mass systems and contributes to most of the BBH population, while formation in dense environments, such as stellar clusters, becomes progressively more important at higher masses.

II. METHODS

With the most recent gravitational wave catalog, GWTC-5 [6] and previous catalogues [81–83], we infer properties of the black hole population using hierarchical Bayesian inference. Detector improvements in GWTC-5 allowed for these new detected events [84–90]. Consistent with previous studies [e.g., 78], we focus on sources with a false alarm rate of $\text{FAR} < 1 \text{ yr}^{-1}$. Filtering by this rate leaves 259 events. Selection effects are accounted for using recovered injections from injection campaigns [91, 92].

We factorize the astrophysical merger-rate density as

$$\mathcal{R}(m_1, m_2, z, \chi_{\text{eff}}) = \mathcal{R}_{\text{ref}} \frac{f(m_1)}{f(20 M_\odot)} \frac{(1+z)^\kappa}{(1.2)^\kappa} p(m_2|m_1)p(\chi_{\text{eff}}|m_1). \quad (2)$$

Here, \mathcal{R}_{ref} is the source-frame merger-rate density per unit primary mass at $m_1 = 20 M_\odot$ and $z = 0.2$, m_2 is the secondary mass, and κ controls the redshift evolution of the intrinsic volumetric merger rate. The factor $(1.2)^\kappa$ normalizes the redshift evolution to unity at the reference redshift $z = 0.2$.

The primary mass spectrum is modeled non-parametrically using a Gaussian process (hereafter \mathcal{GP}). We assume a zero-mean \mathcal{GP} with a squared-exponential covariance kernel, such that

$$f(m_1) = \exp[\Phi(\ln m_1)], \quad (3)$$

with

$$\Phi(\ln m_1) \sim \mathcal{GP}(0, k(x, x'; a_{m_1}, l_{m_1})) \quad (4)$$

and

$$k(x, x'; a_{m_1}, l_{m_1}) = a_{m_1}^2 \exp\left[-\frac{(x - x')^2}{2l_{m_1}^2}\right]. \quad (5)$$

The \mathcal{GP} is evaluated on a log-uniform grid in primary mass over the range 2–200 M_\odot .

We similarly model the secondary-mass distribution conditionally on the primary mass as

$$p(m_2 | m_1) \propto m_2^{\beta_q(m_1)}, \quad (6)$$

where the power-law index β_q is itself allowed to vary with primary mass according to a \mathcal{GP} model,

$$\beta_q(m_1) = \Xi(\ln m_1), \quad (7)$$

with

$$\Xi(\ln m_1) \sim \mathcal{GP}(0, k(x, x'; a_{\beta_q}, l_{\beta_q})). \quad (8)$$

As above, the \mathcal{GP} is constructed with a zero mean and squared-exponential covariance kernel and is evaluated on a log-uniform grid in primary mass between 2 and $200 M_\odot$.

We model the χ_{eff} distribution using a generalized transition model with two characteristic mass scales, \tilde{m}_{low} and \tilde{m}_{high} , allowing us to isolate spin populations within a finite interval of primary mass. The effective-spin distribution conditioned on primary mass is written as

$$p(\chi_{\text{eff}} | m_1) = p_{\text{out}}(\chi_{\text{eff}} | m_1) [1 - \zeta(m_1)] + p_{\text{in}}(\chi_{\text{eff}} | m_1) \zeta(m_1), \quad (9)$$

where p_{in} describes the spin population between the two transition masses and p_{out} describes the population outside this interval. The mixing function is defined as

$$\zeta(m_1) = \frac{1}{1 + \exp\left[\frac{-(m_1 - \tilde{m}_{\text{low}})}{M_\odot}\right]} \left[1 - \frac{1}{1 + \exp\left[\frac{-(m_1 - \tilde{m}_{\text{high}})}{M_\odot}\right]} \right]. \quad (10)$$

In this construction, $\zeta(m_1) \simeq 1$ for $\tilde{m}_{\text{low}} \lesssim m_1 \lesssim \tilde{m}_{\text{high}}$ and $\zeta(m_1) \simeq 0$ outside this interval. This generalized model therefore allows us to probe whether the effective-spin distribution changes within selected regions of the BBH mass spectrum.

The spin component p_{in} is modeled non-parametrically as

$$p_{\text{in}}(\chi_{\text{eff}} | m_1) = \frac{\mathcal{H}(\chi_{\text{eff}}) e^{\Theta(\chi_{\text{eff}})}}{\int_{-1}^1 \mathcal{H}(\chi_{\text{eff}}) e^{\Theta(\chi_{\text{eff}})} d\chi_{\text{eff}}}, \quad (11)$$

where $\Theta(\chi_{\text{eff}})$ is modeled using a Gaussian process and $\mathcal{H}(\chi_{\text{eff}})$ is a Heaviside window function defining the support of the distribution,

$$\mathcal{H}(\chi_{\text{eff}}) = \begin{cases} 1 & \chi_{\text{min}} \leq \chi_{\text{eff}} \leq \chi_{\text{max}} \\ 0 & \text{otherwise} \end{cases}. \quad (12)$$

This construction allows the minimum and maximum extent of each inferred χ_{eff} distribution to vary freely and be constrained directly by the data. The parameters χ_{min} and χ_{max} are sampled independently for each population from the priors described in Table S1. In particular, the lower bound is sampled conditionally on the upper bound according to

$$\pi(\chi_{\text{min}} | \chi_{\text{max}}) = \chi_{\text{min,unscaled}}(\chi_{\text{max}} + 1) - 1. \quad (13)$$

The spin component outside the interval is modeled as a mixture of a Normal and a uniform distribution;

$$p_{\text{out}}(\chi_{\text{eff}} | m_1) = \mathcal{N}(\chi_{\text{eff}}; \mu, \sigma)\xi + \quad (14)$$

$$\mathcal{U}(\chi_{\text{eff}}; \chi_{\text{min,out}}, \chi_{\text{max,out}})(1 - \xi), \quad (15)$$

where \mathcal{U} represents a uniform distribution with independent bounds, and \mathcal{N} is a truncated normal distribution. The quantities μ , σ , χ_{min} , and χ_{max} are free parameters and sample according to Table S1. Since our primary interest is the population within the interval, these nuisance parameters are marginalized over but are not otherwise discussed or reported in this work.

An important feature of this construction is that it allows the inferred distribution to approach arbitrarily small values over parts of parameter space if required by the data, i.e., very small (near zero) probabilities at certain points. This provides more flexibility than commonly adopted parametric or spline-based models, which often enforce a non-zero density everywhere or impose a fixed functional form on the spin distribution. Our approach therefore enables the identification of localized features and disconnected support in the χ_{eff} distribution that may arise from distinct astrophysical formation processes.

III. RESULTS

A. Mass dependent mass-ratio distribution

We first focus on the dependence of the mass-ratio distribution as a function of primary mass. Figure 1 shows the differential merger-rate density (top panel) together with the inferred slope $\beta(m_1)$ of the conditional mass-ratio distribution (middle panel). The main result of this analysis is the emergence of four distinct mass regions characterized by different mass-ratio distributions, which are shown in Figure 2.

At low masses, $m_1 \lesssim 15 M_\odot$, the inferred slope satisfies $\beta \gtrsim 2$ at 90% credibility, indicating a strong preference for nearly equal-mass binaries. This region coincides with the first peak in the merger-rate distribution around $10 M_\odot$.

In the mass range $18\text{--}30 M_\odot$, the inferred mass-ratio distribution becomes substantially flatter, with β consistent with the interval $-1 \lesssim \beta \lesssim 1$. This behavior is inconsistent with the low-mass population at approximately the 90% confidence level and coincides with a plateau-like feature in the merger-rate density.

At intermediate masses, within the interval $30\text{--}50 M_\odot$, the population transitions back to a regime favoring equal-mass binaries, with $\beta \gtrsim 2$ once again preferred at 90% confidence. This interval is associated with a possible secondary peak in the merger-rate distribution near $35 M_\odot$ seen in the mass distribution.

Finally, above approximately $50 M_\odot$, the inferred mass-ratio distribution flattens again, with β returning to values consistent with $-1 \lesssim \beta \lesssim 1$. The inferred values of β in this regime are statistically consistent with those found between $15\text{--}30 M_\odot$, but inconsistent with the more equal-mass populations inferred below $\sim 15 M_\odot$ and between $30\text{--}50 M_\odot$. This transition occurs near the sharp decline in the merger-rate density beginning at $\sim 40 M_\odot$,

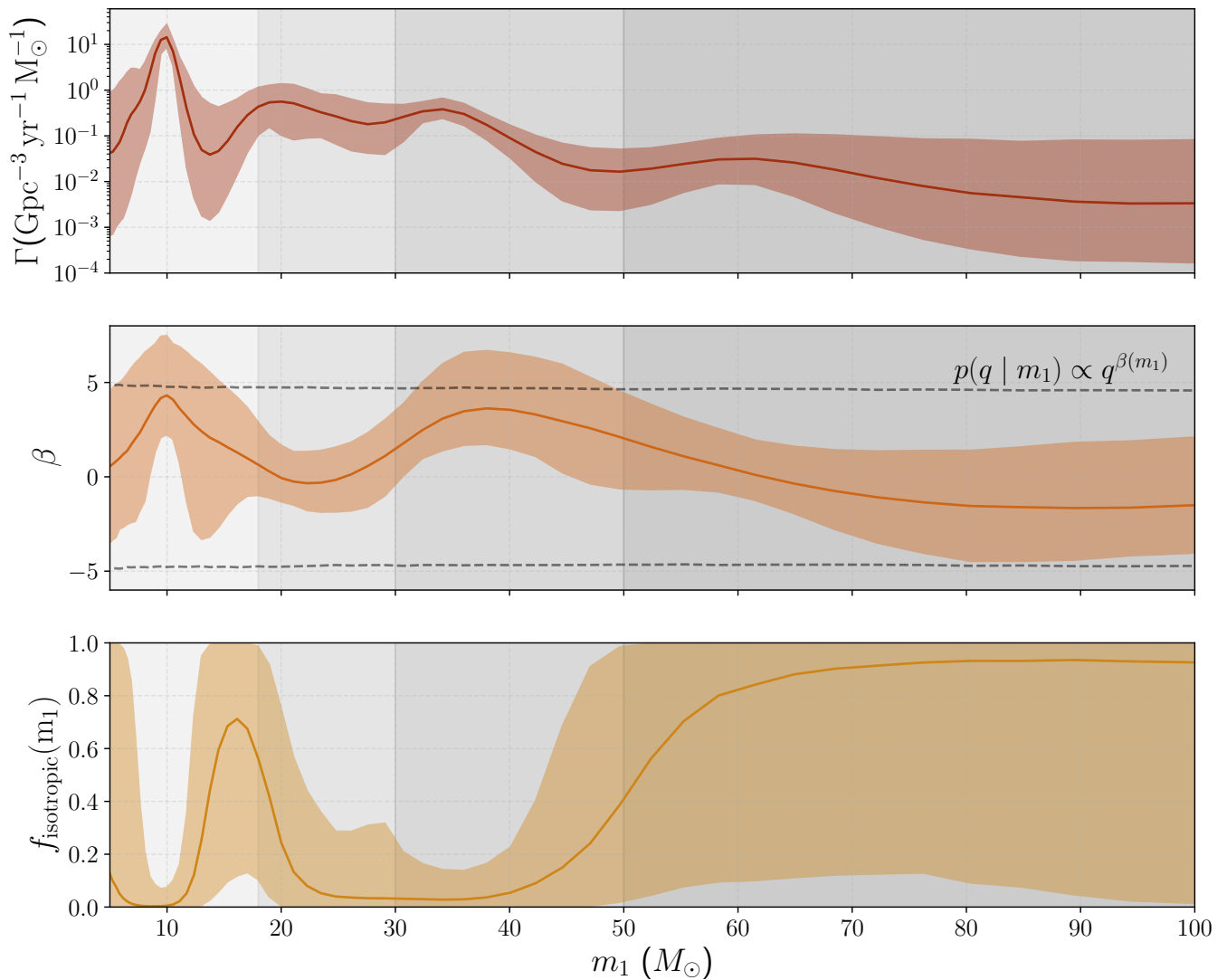


Figure 1. Top panel: Γ is the astrophysical/source-frame merger-rate density per unit primary mass as a function of primary mass m_1 . Middle panel: inferred slope $\beta(m_1)$ of the conditional mass-ratio distribution, $p(q | m_1) \propto q^{\beta(m_1)}$, obtained using our Gaussian-process population model. The dashed lines in this panel are the 90% confidence bands of the prior on $\beta(m_1)$. Bottom panel: inferred mixing fraction of an isotropic spin population from the LVK analysis of Ref. [7], based on a model in which the χ_{eff} distribution is described as a mixture between a Gaussian component and a broad uniform component, with the mixing fraction modeled as a Gaussian process as a function of mass. Vertical shaded bands indicate the mass intervals discussed in the text. Colored shaded regions show 90% intervals, while the solid lines are the inferred median. Here we set $(\tilde{m}_{\text{low}}, \tilde{m}_{\text{high}}) = (50, 200)M_\odot$. However, the mass and q distributions shown here were found to be independent of the choice for these parameters.

which is followed by a broad high-mass plateau.

For comparison, the lower panel of Fig. 1 shows the inferred mixing fraction of an isotropic spin population from the LIGO–Virgo–KAGRA collaboraton (LVK) analysis of Ref. [7], based on the model we introduced in Ref. [22]. In that framework, the χ_{eff} distribution is described as a mixture between a Gaussian component and a broad uniform distribution extending over $|\chi_{\text{eff}}| < 0.5$, intended to represent an isotropic spin population such as might arise from hierarchical mergers. The mixing fraction between these two components is itself modeled

as a Gaussian process as a function of primary mass.

The transitions identified in $\beta(m_1)$ approximately coincide with mass intervals where the inferred isotropic spin fraction increases or decreases. In particular, in the flatter mass-ratio region above $50 M_\odot$, the isotropic component is inferred to have a non-zero contribution at the 90% confidence level. By contrast, in the intermediate mass ranges, where the population favors nearly equal-mass binaries, the isotropic fraction is constrained to remain at the level of $\lesssim 10\%$. At lower masses, the population below $\sim 20 M_\odot$ is largely dominated by a low-

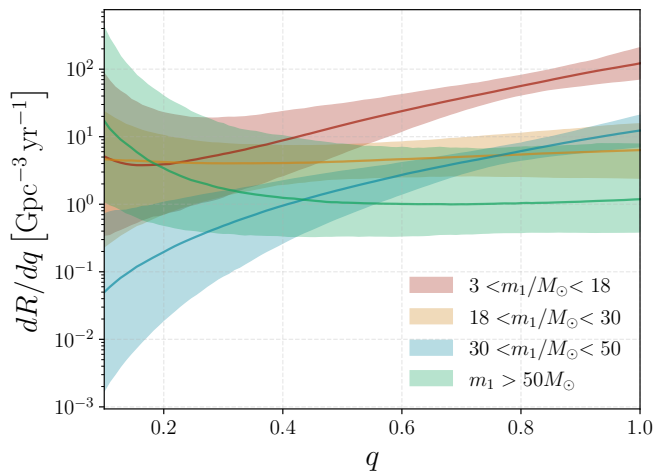


Figure 2. The merger rate as a function of mass ratio q for each mass interval. The shaded region represents the 90% confidence interval and the solid line is the median. Intervals $18 < m_1/M_\odot < 30$ and $m_1 > 50M_\odot$ show a flattening in the merger rate in comparison to $m_1 < 18M_\odot$ and $30 < m_1/M_\odot < 50$.

spin component with $f_{\text{isotropic}} \simeq 0$. However, toward the upper edge of this interval, a secondary isotropic component becomes visible, consistent with features previously identified in other studies [22, 73, 93]. This increase in the isotropic fraction coincides with a local dip in the merger-rate density, implying that this component contributes only a small fraction of the overall merger rate in this mass range.

Early LVK population analyses of GWTC-1 and GWTC-2 modeled the mass-ratio distribution using a single power law, $p(q) \propto q^\beta$, and generally inferred positive values of β , consistent with a preference for nearly equal-mass binaries [94]. This is consistent with our inference favoring large values of β near $m_1 \sim 10M_\odot$, where most of the astrophysical population is clustered. The GWTC-3 and GWTC-4 population analysis similarly found that the observed BBH population is dominated by comparable-mass systems, while also identifying confidently unequal-mass mergers such as GW190412 and GW190517_055101 [11, 95]. However, these analyses largely assumed a smooth or weakly varying mass-ratio distribution across the full mass range.

The latest LVK GWTC-5 population analysis [7] has identified evidence for more complex mass-dependent structure in the BBH population. In particular, that analysis reports that the feature near $35M_\odot$ is dominated by nearly equal-mass binaries, while the population above $45M_\odot$ exhibits substantially broader mass-ratio distributions. These results suggest that the shape of $p(q)$ evolves significantly across the primary-mass spectrum and that the BBH population may not be well described by a single smooth mass-ratio model.

This emerging picture is further supported by recent independent analyses. More recently, several studies

have begun to identify evidence for multiple BBH subpopulations with distinct mass-ratio properties [70, 71, 96, 97]. Ref. [71] found evidence for at least three BBH subpopulations separated by transitions in primary mass, including an intermediate-mass population strongly peaked toward equal masses and a high-mass population with broader mass-ratio distributions and larger spins. Ref. [70] reached qualitatively similar conclusions using parametrized mixture models, arguing that the peak near $10M_\odot$ and the feature near $35M_\odot$ correspond to distinct populations with different mass-ratio and spin properties, while the highest-mass systems are associated with flatter mass-ratio distributions consistent with hierarchical mergers.

Our analysis supports the results of previous and concurrent work. In particular, we recover evidence that the $35M_\odot$ feature is associated with a population strongly favoring equal-mass binaries, as seen in [7, 70, 95, 98–104]. Meanwhile, the population above $\sim 45\text{--}50M_\odot$ exhibits substantially flatter mass-ratio distributions, consistent with the results of Refs. [70] and [71]. However, we also find that the low-mass BBH population itself separates into two statistically distinct regimes: a component below $\sim 15M_\odot$ characterized by strongly equal-mass binaries with $\beta \gtrsim 2$, and a second component between $\sim 15\text{--}30M_\odot$ with substantially flatter mass-ratio distributions, $-1 \lesssim \beta \lesssim 1$. Our analysis therefore favors at least four distinct mass regimes separated by transitions in the mass-ratio distribution. These transitions coincide with structures in the primary-mass spectrum, including the peak near $10M_\odot$, the plateau between $15\text{--}30M_\odot$, the feature near $35M_\odot$, and the high-mass tail above $50M_\odot$.

B. Mass-dependent effective-spin distribution

We consider four population models in the following mass intervals:

$$(\tilde{m}_{\text{low}}, \tilde{m}_{\text{high}}) = (3, 18) M_\odot,$$

$$(\tilde{m}_{\text{low}}, \tilde{m}_{\text{high}}) = (18, 30) M_\odot,$$

$$(\tilde{m}_{\text{low}}, \tilde{m}_{\text{high}}) = (30, 50) M_\odot,$$

$$(\tilde{m}_{\text{low}}, \tilde{m}_{\text{high}}) = (50, 200) M_\odot,$$

representing the four regions identified from the mass-ratio analysis in Figure 1. Computing how many events contain at least 10% of their primary mass posterior samples in each interval leaves 67 events in the $(3, 18)M_\odot$ range, 85 in $(18, 30)M_\odot$, 156 in $(30, 50)M_\odot$, and 81 events for $(50, 200)M_\odot$. The inferred effective-spin distributions are given in Figure 3. The inferred PDFs in adjacent mass intervals show localized regions of strong posterior separation, with the density within and below/above

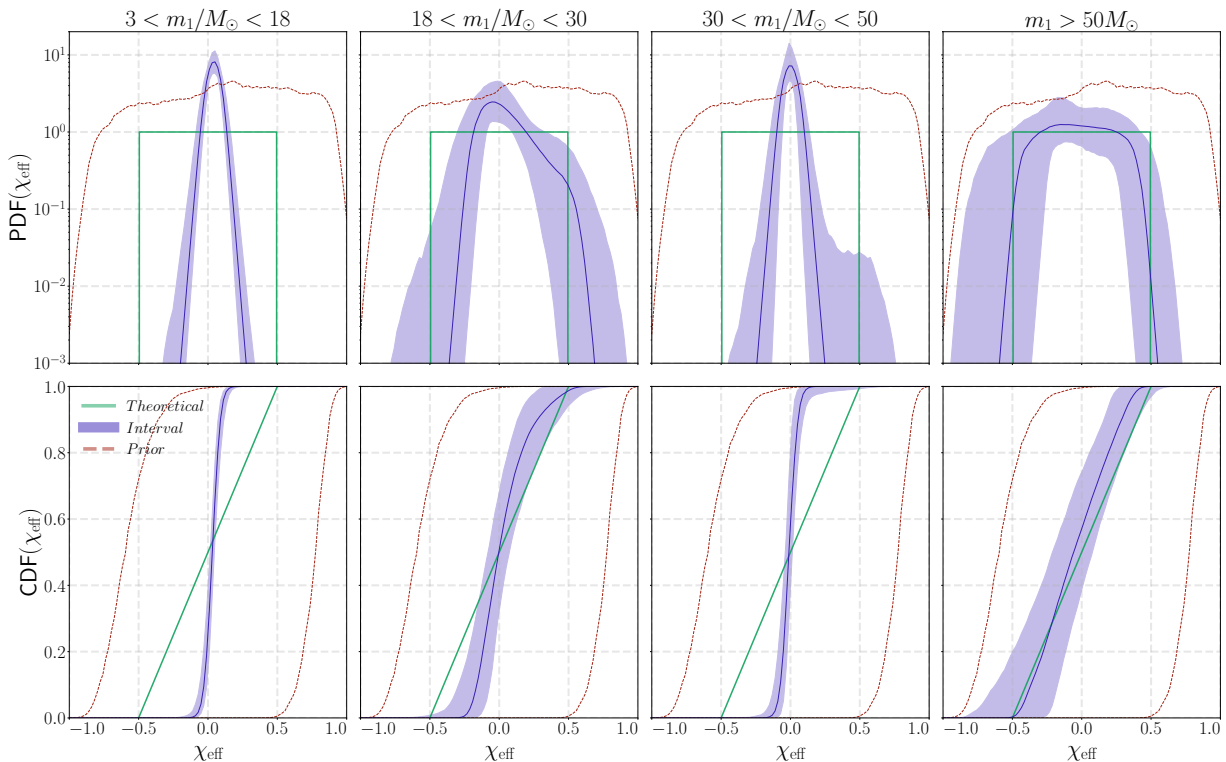


Figure 3. Inferred effective-spin distributions across the four mass intervals identified from the mass-ratio analysis: $m_1 < 18 M_\odot$, $18 < m_1/M_\odot < 30$, $30 < m_1/M_\odot < 50$, and $m_1 > 50 M_\odot$. The top panels show the probability density functions and the bottom panels the corresponding cumulative distributions. Shaded regions show the 90% confidence intervals, and solid lines the recovered median distribution. Red dotted lines show the prior ranges. The green lines indicate the distribution expected if the population formed hierarchically in dense clusters. The four intervals exhibit alternating narrow and broad spin populations, with the $m_1 < 18 M_\odot$ and $30 < m_1/M_\odot < 50$ populations characterized by narrow distributions, while the $18 < m_1/M_\odot < 30$ and $m_1 > 50 M_\odot$ intervals show substantially broader support extending toward both positive and negative effective spins.

the mass transition differing at $> 99\%$ posterior probability at some values of χ_{eff} . As a robustness check, in the Supplemental Material we also consider an alternative set of models with a single mass transition whose location is varied across the mass spectrum. This additional analysis shows that the main qualitative conclusions described in what follows are likely to be insensitive to the specific binning adopted here.

The lowest-mass interval, $m_1 \lesssim 18 M_\odot$, is characterized by a narrow χ_{eff} distribution peaked at small positive values, with little evidence for extended tails. The distribution is approximately symmetric and closely resembles the population-averaged spin distribution inferred in previous LVK analyses, consistent with the fact that the majority of the BBH mergers in the astrophysical population are concentrated near the $10 M_\odot$ peak and therefore dominate population-averaged measurements. In this mass interval, the 5th percentile of the cumulative distribution function evaluated at zero lies above 0.15, implying that more than 15% of the population has negative effective spin at 95% credibility.

In the second interval, $18 \lesssim m_1/M_\odot \lesssim 30$, the inferred χ_{eff} distribution changes significantly. The distribution

becomes consistent with being centered at $\chi_{\text{eff}} \simeq 0$ and develops broader support toward both positive and negative values, together with a possible excess of positive $\chi_{\text{eff}} \simeq 0.5$ systems or a positive skewness. Owing to the increased width of the distribution, however, the associated uncertainties grow significantly, and positive values of the median comparable to those inferred for the $m_1 \lesssim 18 M_\odot$ population cannot be ruled out. In the $18 \lesssim m_1/M_\odot \lesssim 30$ mass interval, we find that more than 32% of the population has negative effective spin at 95% credibility.

The third interval, $30 \lesssim m_1/M_\odot \lesssim 50$, transitions back to a narrow χ_{eff} distribution. In contrast to the first interval, however, the distribution is now sharply peaked around $\chi_{\text{eff}} \simeq 0$ rather than at positive values. The median and mean 90% credible intervals do not overlap with those inferred for the lower-mass population, providing strong evidence that the two populations are statistically distinct. Remarkably, the width of the distribution in this mass interval is nearly identical to that inferred for the $m_1 \lesssim 18 M_\odot$ population. This may suggest that both populations are predominantly composed of first-generation black holes formed through sim-

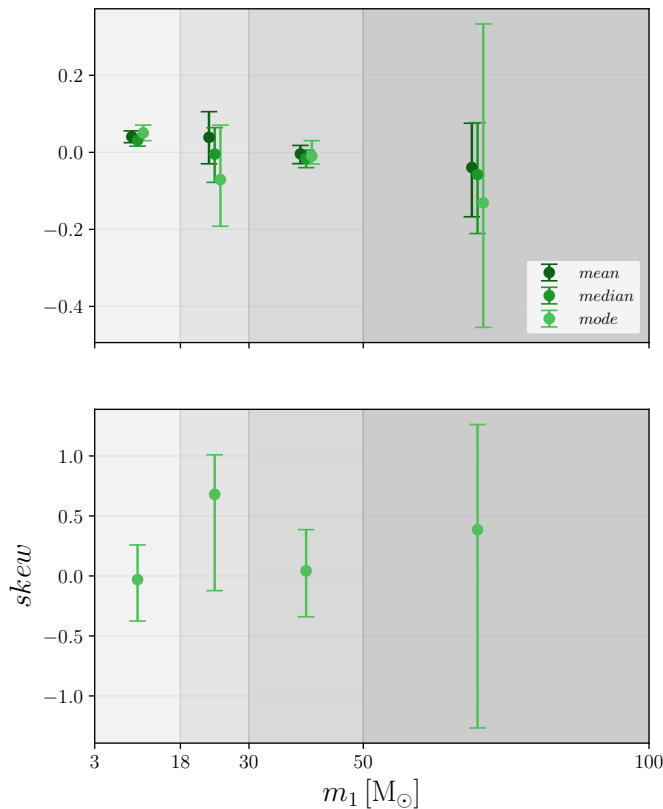


Figure 4. Summary statistics of the inferred effective-spin distributions across the four mass intervals identified from the mass-ratio analysis: $m_1 < 18 M_\odot$, $18 < m_1/M_\odot < 30$, $30 < m_1/M_\odot < 50$, and $m_1 > 50 M_\odot$. Error bars indicate the 90% credible intervals. The upper panel shows the mean, median, and mode of the inferred χ_{eff} distributions, while the lower panel shows the corresponding Pearson first skewness coefficient. The latter is computed with respect to the mode of the distribution.

ilar stellar-evolution processes, while differing primarily in the mechanism through which binaries are assembled and merged. In particular, the higher-mass population may contain a larger contribution from dynamical assembly channels, naturally leading to more isotropic spin orientations despite retaining similarly narrow intrinsic spin magnitudes. In the $30 \lesssim m_1/M_\odot \lesssim 50$ mass interval, we find that more than 39% of the population has negative effective spin at 95% credibility.

Finally, the highest-mass interval, $m_1 \gtrsim 50 M_\odot$, exhibits the broadest spin distribution, with support extending across a large fraction of the allowed χ_{eff} range. The corresponding cumulative distribution becomes substantially flatter and consistent with expectations for an isotropic-spin population associated with hierarchical mergers. In this highest mass interval we infer that more than 39% of the population has negative effective spin at 95% credibility.

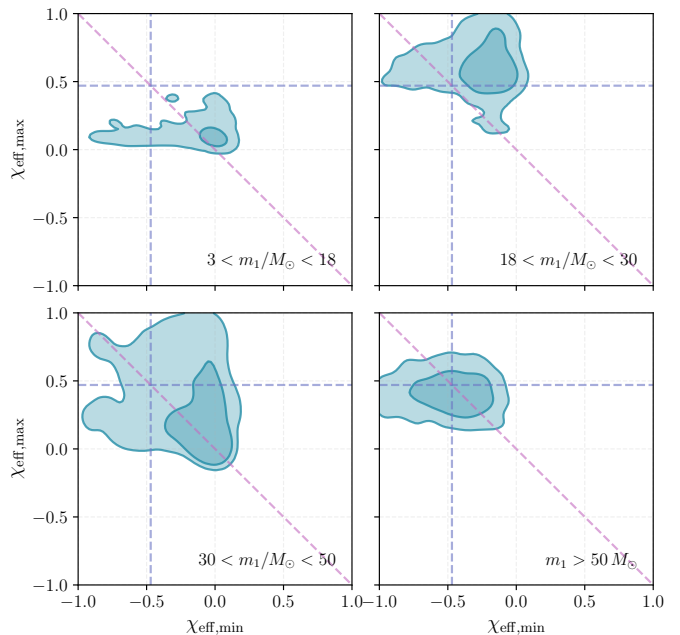


Figure 5. Posterior support for the minimum and maximum extent of the inferred effective-spin distributions across the four mass intervals identified from the mass-ratio analysis: $m_1 < 18 M_\odot$, $18 < m_1/M_\odot < 30$, $30 < m_1/M_\odot < 50$, and $m_1 > 50 M_\odot$. Contours at 95% and 68% confidence show the inferred joint posterior on $\chi_{\text{eff,min}}$ and $\chi_{\text{eff,max}}$ for each interval. The low-mass population is strongly concentrated toward small values of $\chi_{\text{eff,max}}$, while the higher-mass intervals exhibit progressively broader support extending toward larger positive and negative effective spins. The blue dashed lines indicate $\chi_{\text{eff,min}} = -0.47$ and $\chi_{\text{eff,max}} = 0.47$, approximately corresponding to the characteristic support expected from hierarchical mergers. Since for $m_1 < 18 M_\odot$, the expected value lies outside the population 90% contours, in this mass range the data do not require a subdominant population of hierarchical mergers. A possible contribution is not excluded in any of the higher mass intervals. The pink dashed line marks the locus $y = -x$, corresponding to support intervals that are symmetric about $\chi_{\text{eff}} = 0$.

1. Distribution symmetry

Non-Gaussian features in the χ_{eff} distribution like skewness, asymmetry about zero, and multimodality can naturally arise in the χ_{eff} distribution if multiple channels are contributing to the detected population [105]. Thus, in this section we further investigate the symmetry of the recovered χ_{eff} distributions. In Figure 4 we show the mean, median, and mode of the distributions, while the lower panel shows the Pearson first skewness coefficient, $\gamma_P = \frac{\mu - \text{Mode}}{\sigma}$, where μ and σ are the mean and standard deviation of the distribution. In Table I we report the recovered values for these quantities.

The lowest-mass population exhibits a small but consistently positive mean and median, confirming that the $\sim 10 M_\odot$ population is mildly shifted toward positive

Interval	Mean	Median	Mode	Skew
$m_1 < 18 M_\odot$	$0.041^{+0.02}_{-0.02}$	$0.031^{+0.01}_{-0.02}$	$0.051^{+0.02}_{-0.02}$	$-0.030^{+0.29}_{-0.35}$
$18 < m_1/M_\odot < 30$	$0.039^{+0.07}_{-0.07}$	$-0.005^{+0.07}_{-0.07}$	$-0.071^{+0.14}_{-0.12}$	$0.680^{+0.33}_{-0.80}$
$30 < m_1/M_\odot < 50$	$-0.004^{+0.02}_{-0.03}$	$-0.016^{+0.02}_{-0.02}$	$-0.010^{+0.04}_{-0.02}$	$0.043^{+0.34}_{-0.38}$
$m_1 > 50 M_\odot$	$-0.039^{+0.11}_{-0.13}$	$-0.058^{+0.13}_{-0.15}$	$-0.131^{+0.46}_{-0.32}$	$0.386^{+0.88}_{-1.65}$

Table I. Results of summary statistics from the effective spin distribution for each mass interval. These are shown graphically in Figure 4.

χ_{eff} . At the same time, the skewness remains consistent with zero, indicating that the distribution is symmetric around its peak. The broader 18–30 M_\odot population shows tentative evidence for positive skewness, consistent with a possible excess near positive χ_{eff} discussed above, although a symmetric distribution remains fully consistent with the data. The 30–50 M_\odot interval is narrowly distributed and centered at $\chi_{\text{eff}} \simeq 0$, despite having a width comparable to that of the lowest mass population. The highest-mass interval exhibits substantially larger uncertainties, primarily because the inferred distribution is much broader, making asymmetries difficult to constrain. Overall, all four mass intervals remain statistically consistent with symmetric χ_{eff} distributions.

We now return to the origin of the possible skew toward positive values of χ_{eff} within the 18–30 M_\odot mass region. A similar feature was identified in concurrent studies [106]. One possible interpretation is that this feature reflects the emergence of a subpopulation of hierarchical mergers, since remnants from previous mergers are expected to have dimensionless spins of order ~ 0.7 , naturally producing systems with large spins and $\chi_{\text{eff}} \lesssim 0.5$ when partially aligned with the orbital angular momentum. However, we caution that such a feature is intrinsically difficult to measure robustly. Spin measurements are subject to large statistical uncertainties [107–113], and the mass-ratio–spin degeneracy can bias the inferred χ_{eff} of individual systems toward positive values [114–118]. In addition, selection effects preferentially enhance the detectability of systems with large positive χ_{eff} while disfavoring systems with negative χ_{eff} [118–120]. These effects can make a broad underlying spin distribution appear skewed toward positive χ_{eff} , particularly when the number of events contributing in a given mass interval is small. Our hierarchical Bayesian analysis accounts for selection effects at the population level, and finds that the distribution is consistent with being symmetric. Consequently, the apparent tail towards positive χ_{eff} may reflect a broader isotropic or hierarchical-merger population whose negative-spin counterpart is more difficult to resolve observationally.

2. Constraints on hierarchical merger populations

Figure 5 further illustrates the qualitative differences between the four mass intervals through the inferred support of the effective-spin distributions. The low-mass

population, $m_1 < 18 M_\odot$, is strongly concentrated toward small values of both $\chi_{\text{eff,min}}$ and $\chi_{\text{eff,max}}$, with little support for extended positive-spin tails. In particular, the data disfavor broad spin distributions extending toward $\chi_{\text{eff,max}} \gtrsim 0.5$, indicating that current observations do not require a significant contribution from hierarchical mergers to the dominant low-mass population. The absence of a broad high-spin component below 18 M_\odot therefore suggests that the 10 M_\odot peak is primarily composed of first-generation binaries formed through channels producing relatively small spins with a mild preference for aligned systems.

By contrast, the higher-mass intervals show progressively broader support extending toward larger values of $\chi_{\text{eff,max}}$, especially for $18 < m_1/M_\odot < 30$ and $m_1 > 50 M_\odot$. These regions are more compatible with populations containing hierarchical mergers or isotropic-spin systems. In particular, the data do not exclude the presence of binaries whose components are themselves remnants of previous black hole mergers.

Figure 6 illustrates how the inferred χ_{eff} distribution for $m_1 \gtrsim 45 M_\odot$ compares with expectations for hierarchical mergers and how the observational constraints have improved from GWTC-3 to GWTC-5. This distribution was obtained as in the other models setting $(\tilde{m}_{\text{low}}, \tilde{m}_{\text{high}}) = (45, 200) M_\odot$. We set $\tilde{m}_{\text{low}} = 45 M_\odot$ as this is a value close to the mass transition obtained in previous work [26, 68, 121], allowing for direct comparison with the literature. The upper panel shows the inferred support of the minimum and maximum extent of the χ_{eff} distribution obtained from successive gravitational-wave catalogs.

The upper bound of the distribution, $\chi_{\text{eff,max}}$, is now well constrained and remains consistent with the values expected from hierarchical mergers. At the same time, the lower bound $\chi_{\text{eff,min}}$ is becoming increasingly constrained as the catalog grows, with the posterior now excluding both $\chi_{\text{eff,min}} = -1$ and $\chi_{\text{eff,min}} = 0$ at 99% confidence. This indicates that the observed high-mass population is fully consistent with a pure hierarchical formation scenario.

The lower panel directly compares the inferred χ_{eff} distributions below and above the transition mass scale \tilde{m} . The low-mass population remains sharply peaked around small positive values of χ_{eff} with very limited support for broad tails, while the high-mass population develops substantially broader support extending toward both positive and negative effective spins. Overall, these results

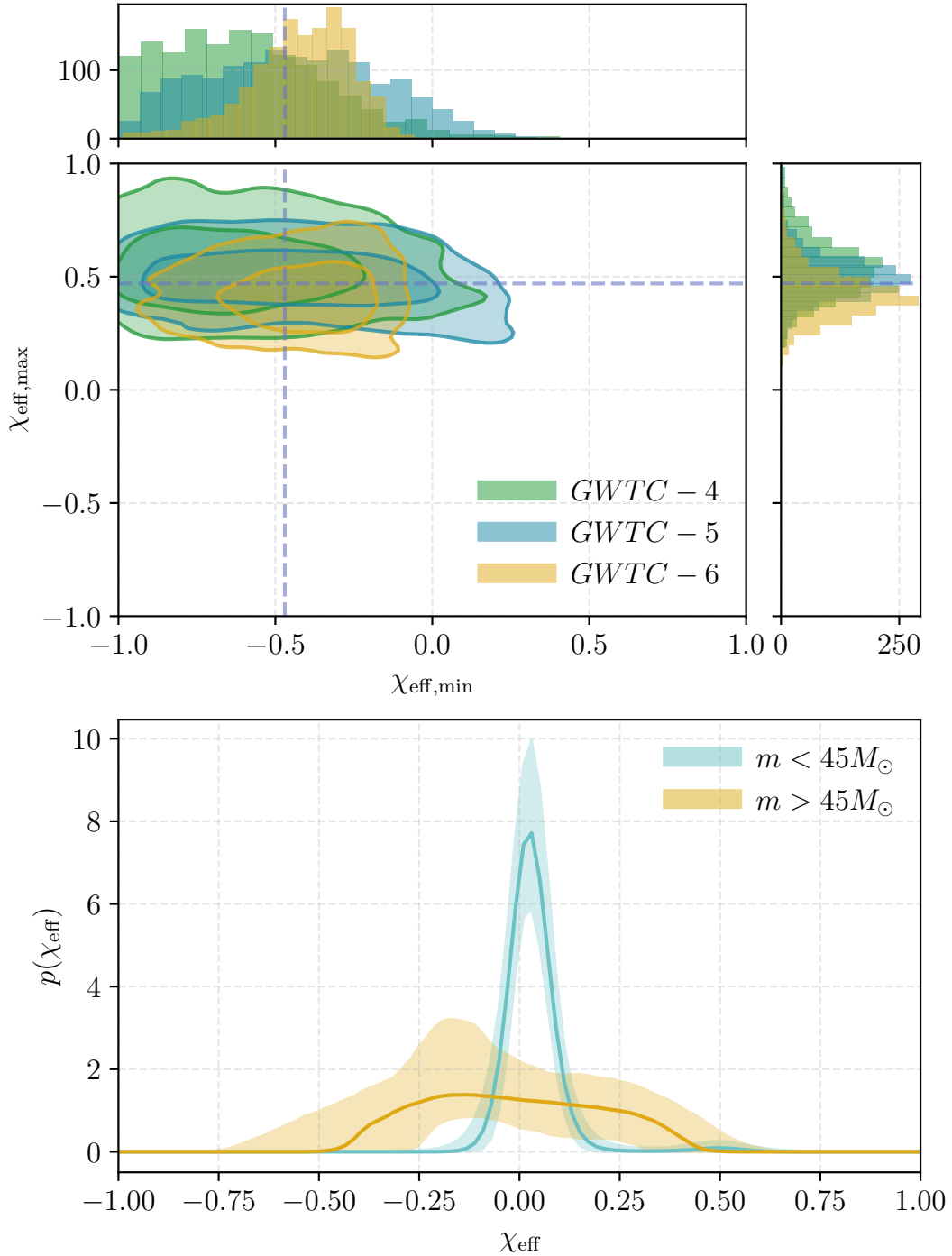


Figure 6. Comparison between the inferred effective-spin support of the high-mass BBH population and the expectations for hierarchical mergers. The upper panel shows the joint posterior on $\chi_{\text{eff,min}}$ and $\chi_{\text{eff,max}}$ inferred from GWTC-3, GWTC-4, and GWTC-5 for the high-mass population above the transition mass scale $\tilde{m} = 45M_{\odot}$. The corresponding marginalized distributions are shown along the top and right panels. With the increase of the catalog size, the constraints on the extent of the χ_{eff} distribution have improved substantially. The data favor $\chi_{\text{eff,max}} \sim 0.5$ and increasingly constrain $\chi_{\text{eff,min}}$ toward values near -0.5 , while strongly disfavoring both $\chi_{\text{eff,min}} = -1$ and $\chi_{\text{eff,min}} = 0$. The dashed lines indicate $\chi_{\text{eff,min}} = -0.47$ and $\chi_{\text{eff,max}} = 0.47$, corresponding to the characteristic support expected from hierarchical mergers. The lower panel compares the inferred χ_{eff} distributions below and above the transition mass scale \tilde{m} . The low-mass population remains sharply peaked around small positive values of χ_{eff} , while the high-mass population develops substantially broader support extending toward both positive and negative effective spins. The broad support of the high-mass population is consistent with expectations for binaries containing remnants of previous black hole mergers.

are in qualitative agreement with our previous analysis, but the significantly larger GWTC-5 catalog now provides substantially tighter constraints on the allowed extent and asymmetry of the high-mass spin population.

IV. ASTROPHYSICAL INTERPRETATION AND CONCLUSIONS

In this section, we discuss the astrophysical implications of the mass-dependent structure identified in the BBH population. Our analysis reveals multiple sharp transitions in both the mass-ratio and effective-spin distributions as a function of primary mass, suggesting that different regions of the BBH mass spectrum are governed by different binary properties and possibly by different formation scenarios. We consider here whether the transitions identified in $p(q|m_1)$ and $p(\chi_{\text{eff}}|m_1)$ reflect changes in the dominant mechanisms responsible for binary assembly and evolution.

A particularly important result of this work is the strong correlation between changes in the mass-ratio distribution and corresponding changes in the effective-spin distribution. The same mass scales that separate equal-mass and broad mass-ratio populations also coincide with transitions from narrow aligned-spin distributions to broader distributions consistent with isotropic or hierarchical populations. This connection provides further evidence that the evolution of binary mass ratios and spins is closely linked and that both quantities carry complementary information about the astrophysical origin of BBH mergers.

A clear transition occurs near $15 M_\odot$, where the effective-spin distribution shifts from a narrow distribution peaked at positive χ_{eff} to a broader distribution centered near zero. At the same mass scale, the conditional mass-ratio distribution changes from strongly favoring equal-mass binaries to a substantially flatter distribution. Together, these results indicate that the population associated with the $10 M_\odot$ peak is statistically distinct from the population dominating at higher masses.

The low-mass population is characterized by relatively small spins with a mild preference for positive χ_{eff} , while still retaining significant support at negative values. Such a distribution might be achieved with standard isolated binary evolution models. In isolated binary evolution, tidal synchronization, mass transfer, and common-envelope interactions tend to align stellar spins with the orbital angular momentum prior to collapse, naturally producing BBHs with preferentially positive χ_{eff} [122–125]. At the same time, binary stellar evolution naturally favors nearly equal-mass systems because mass transfer and common-envelope evolution efficiently drive binaries toward comparable component masses [38, 126–128]. Natal kicks during compact-object formation or/and inefficient tides can nevertheless result in significant spin-orbit misalignment, broadening the χ_{eff} distribution and producing some finite support for negative values [122, 123].

Overall, however, matching the narrow mildly positive χ_{eff} distribution of the low-mass population within standard isolated binary evolution models might require non-standard assumptions [123, 129] given the significant fraction of misaligned systems required by the data.

Similarly, triple-mediated formation channels are expected to produce nearly equal-mass binaries since the stellar processes that drive isolated binaries also affect the evolution of the inner binary in a triple system. Although previous work has shown that some fraction of the population may exhibit a broader mass-ratio distribution [130], we note that those models neglected binary interactions, which are the main mechanism expected to drive the preference for equal-mass binaries in this scenario [130]. Secular dynamical interactions in triples can significantly misalign the orbital plane and black-hole spins, naturally producing a population with a mild bias toward positive χ_{eff} while still retaining substantial support for anti-aligned systems [131]. Therefore, triple mediated mergers might also explain the observed distribution [132].

The intermediate region between 18 and $30 M_\odot$ is more difficult to interpret. Here, the population exhibits broader mass-ratio and spin distributions together with tentative evidence for positive skewness and an excess near $\chi_{\text{eff}} \sim 0.5$. Importantly, the inferred positive skewness does not necessarily imply that the population is dominated by positively aligned systems. Instead, the skewness appears to be driven by a possible extended tail toward $\chi_{\text{eff}} \sim 0.5$, while the bulk of the distribution remains concentrated near zero spin. Such a feature may naturally arise from a broader isotropic component associated with hierarchical mergers, whose negative-spin counterpart is more difficult to detect because binaries with positive χ_{eff} remain longer in band and are observationally favored. Consequently, although skewness is possible in this region, the current data remain statistically consistent with a symmetric effective spin distribution (see Fig. 4).

One possibility is therefore that the 18 – $30 M_\odot$ interval represents a transition between the low-mass mildly aligned population and the dynamically assembled populations dominating at higher masses. Alternatively, this region may indicate the emergence of an additional channel, such as mergers embedded in AGN disks [e.g., 56, 106, 133] or the onset of hierarchical mergers below the pair-instability scale [e.g., 96, 134]. In the former scenario, the excess of positive χ_{eff} systems could arise from accretion torques within the AGN disk partially aligning the spins of compact-object binaries with the orbital angular momentum. However, current AGN models do not naturally explain why the distribution would terminate near $\chi_{\text{eff}} \sim 0.5$. By contrast, in the hierarchical-merger interpretation, this characteristic scale arises naturally from the spins expected for merger remnants. In this case, the apparent lack of a corresponding negative- χ_{eff} tail may simply reflect the observational bias against detecting and characterizing anti-aligned systems as dis-

cussed above.

At higher masses, near the feature around $m_1 \simeq 35 M_\odot$, the width of the χ_{eff} distribution is nearly identical to that inferred for the low-mass population below $18 M_\odot$, despite the shift in the location of the peak at zero. This may indicate that both regions are dominated by first-generation black holes formed through similar stellar-evolution processes, while differing primarily in the mechanism through which binaries are assembled. In particular, the $35 M_\odot$ population may naturally arise from dynamical pairing of first-generation black holes in dense stellar clusters [135, 136], producing binaries with small intrinsic spins but nearly isotropic spin-orbit orientations and, possibly, an extended tail representing a subdominant population of hierarchical mergers.

Above $m_1 \simeq 50 M_\odot$, both the mass-ratio and effective-spin distributions broaden substantially. This transition occurs close to the expected onset of the pair-instability mass gap reported in previous studies [137–140] and coincides with the emergence of spin distributions fully consistent with hierarchical mergers. In this regime, repeated mergers in dense stellar clusters may dominate the observed population, naturally producing broader mass-ratio distributions together with effective-spin support extending toward both positive and negative values [141]. The inferred support of the spin distribution is consistent with binaries composed of first- and second-generation black holes [26, 68]. The skewness, mean, median and mode of the χ_{eff} distribution are all consistent with being zero and therefore with an isotropic distribution of spin orientations as expected for dynamical formation in clusters [37].

The breadth of the high-mass effective-spin distribution matches the signature expected from repeated mergers. The remnant of a near-equal-mass merger acquires a nearly universal dimensionless spin peaked at $a \simeq 0.7$, with little support below $a \simeq 0.5$ [142]. For an isotropic distribution of spin orientations, this bounds the effective spin at $|\chi_{\text{eff}}| \lesssim a/1.5 \approx 0.47$ and produces a broad, approximately symmetric distribution [26], in agreement with the support we infer above $50 M_\odot$. The coincidence of this transition with the inferred lower edge of the pair-instability mass gap, $\sim 45 M_\odot$ [22, 23], strengthens the interpretation that the highest-mass systems are predominantly remnants of earlier mergers repopulating the gap.

The fraction of the high-mass population produced hierarchically is governed by the escape velocity of the host environment, which determines whether merger remnants are retained against gravitational-wave recoil [141]. Globular-cluster-like potentials ($v_{\text{esc}} \sim 50 \text{ km s}^{-1}$) retain only a small fraction of remnants, whereas nuclear star clusters ($v_{\text{esc}} \sim 250 \text{ km s}^{-1}$) retain a substantially larger fraction [143]. The relative scarcity of mergers above $50 M_\odot$ therefore limits the contribution of environments

with the highest escape velocities, which would otherwise overproduce massive mergers [144].

We note that while the highest-mass spin distribution is naturally explained within the hierarchical-merger scenario, current data do not exclude distributions that exhibit either a positive or a negative excess of χ_{eff} systems. Alternative formation channels, including stellar evolution with fallback-induced spin-up of the compact remnant [145, 146], stellar mergers [147, 148], chemically homogeneous evolution [149–152], and formation within AGN [55, 56] accretion disks, all provide possible explanations for this population. However, unlike the hierarchical-merger hypothesis, these scenarios do not currently make robust or quantitative predictions for the shape and support of the χ_{eff} distribution, making them considerably more difficult to test directly against gravitational-wave observations.

We thank Charlie Hoy for serving as our internal LVK reviewer. FA and FD are supported by the UK’s Science and Technology Facilities Council grants ST/V005618/1 and UKRI2489. IMRS acknowledges support from the Science and Technology Facilities Council grant number ST/Y001990/1 and the Science and Technology Facilities Council Ernest Rutherford Fellowship grant number UKRI2423. DC acknowledges support from the Gordon and Betty Moore Foundation (Grant GBMF12341). This material is based upon work supported by NSF’s LIGO Laboratory which is a major facility fully funded by the National Science Foundation, as well as the Science and Technology Facilities Council (STFC) of the United Kingdom, the Max-Planck-Society (MPS), and the State of Niedersachsen/Germany for support of the construction of Advanced LIGO and construction and operation of the GEO600 detector. Additional support for Advanced LIGO was provided by the Australian Research Council. Virgo is funded, through the European Gravitational Observatory (EGO), by the French Centre National de Recherche Scientifique (CNRS), the Italian Istituto Nazionale di Fisica Nucleare (INFN) and the Dutch Nikhef, with contributions by institutions from Belgium, Germany, Greece, Hungary, Ireland, Japan, Monaco, Poland, Portugal, Spain. KAGRA is supported by Ministry of Education, Culture, Sports, Science and Technology (MEXT), Japan Society for the Promotion of Science (JSPS) in Japan; National Research Foundation (NRF) and Ministry of Science and ICT (MSIT) in Korea; Academia Sinica (AS) and National Science and Technology Council (NSTC) in Taiwan. This research has made use of data or software obtained from the Gravitational Wave Open Science Center (gwosc.org), a service of the LIGO Scientific Collaboration, the Virgo Collaboration, and KAGRA. The authors are grateful for computational resources provided by Cardiff University and supported by STFC grant ST/V005618/1.

- [1] The LIGO Scientific Collaboration, the Virgo Collaboration, the KAGRA Collaboration, A. G. Abac, A. Abe, I. Abouelfettouh, F. Acernese, K. Ackley, A. Adam, S. Adhichary, D. Adhikari, R. X. Adhikari, V. K. Adkins, S. Afroz, A. Agapito, D. Agarwal, M. Agathos, N. Aggarwal, S. Aggarwal, O. D. Aguiar, I.-L. Ahrend, L. Aiello, A. Ain, P. Ajith, T. Akutsu, L. Albers, W. Ali, S. Al-Kersh, C. Allene, A. Allocca, S. Al-Shammari, J. A. Alvarez, S. Alvarez-Lopez, W. Amar, O. Amarasinghe, A. Amato, F. Amicucci, C. Amra, A. B. Anand, C. Anand, A. Ananyeva, S. B. Anderson, W. G. Anderson, M. Andia, M. Ando, F. Andrade-Oliveira, M. Andrés-Carasona, J. L. Andrey, T. Andrić, J. Anglin, J. Anna, J. M. Antelis, S. Antier, T. Aoki, M. Aoumi, E. Z. Appavuravther, E. A. Appelt, S. Appert, S. K. Apple, K. Arai, A. Araya, M. C. Araya, M. Arca Sedda, F. Arciprete, J. S. Areeda, N. Aritomi, F. Armato, S. Armstrong, N. Arnaud, M. Arogeti, S. M. Aronson, G. Ashton, Y. Aso, L. Asprea, M. Assiduo, S. Assis de Souza Melo, S. M. Aston, P. Astone, P. S. Aswathi, F. Attadio, F. Aubin, K. AultONeal, G. Avalone, N. Avdeev, E. A. Avila, S. Babak, C. Badger, S. Bae, S. Bagnasco, S. Baimukhametova, L. Baiotti, T. Baka, K. A. Baker, T. Baker, G. Balbi, G. Baldi, N. Baldicchi, M. Ball, G. Ballardín, M. Ballelli, S. W. Ballmer, S. Banagiri, B. Banerjee, D. Bankar, T. M. Baptiste, P. Baral, M. Baratti, J. C. Barayoga, K. Baric, B. C. Barish, D. Barker, N. Barman, F. Barone, B. Barr, M. Barrios, L. Barsotti, M. Barsuglia, D. Barta, M. A. Barton, I. Bartos, A. Basalae, R. Bassiri, A. Basti, M. Bawaj, J. C. Bayley, A. C. Baylor, P. A. Baynard, II, M. Bazzan, V. M. Bedakihale, F. Beirnaert, M. Bejger, A. S. Bell, C. Bellani, D. S. Bellie, D. Beltran-Martinez, E. Benedetti, W. Benoit, I. Bentara, M. Ben Yaala, S. Bera, F. Bergamin, B. K. Berger, M. Beroiz, C. P. L. Berry, I. Berry, D. Bersanetti, T. Bertheas, A. Bertolini, J. Betzwieser, D. Beveridge, N. Bevis, J. Bezerra-Sobrinho, R. Bhandare, R. Bhatt, A. Bhattacharjee, D. Bhattacharjee, S. Bhattacharyya, S. Bhau-mik, V. Biancalana, F. Bianchi, I. A. Bilenko, M. Bilicki, G. Billingsley, A. Binetti, S. Bini, S. Biot, O. Birnholtz, S. Biscoveanu, A. Bisht, M. Bitossi, M.-A. Bizouard, S. Blaber, J. K. Blackburn, L. A. Blagg, C. D. Blair, D. G. Blair, M. Bloch, N. Bode, N. Boettner, P. Bogdan, G. Boileau, M. Boldrini, G. N. Bolingbroke, L. D. Bonavena, V. A. Bonhomme, E. Bonilla, M. S. Bonilla, A. Bonino, R. Bonnand, A. Borchers, N. Borghi, V. Boschi, S. Bose, V. Bossilkov, Y. Bothra, A. Boudon, T. D. Boybeyi, M. Boyle, A. Bozzi, and C. Bradaschia, GWTC-5.0: An Introduction to Version 5.0 of the Gravitational-Wave Transient Catalog, arXiv e-prints , arXiv:2605.27223 (2026), arXiv:2605.27223 [gr-qc].
- [2] T. L. S. Collaboration, the Virgo Collaboration, and the KAGRA Collaboration, Gwtc-5.0: Methods for identifying and characterizing gravitational-wave transients (2026), arXiv:2605.27224 [gr-qc].
- [3] Abbott et al., GWTC-1: A Gravitational-Wave Transient Catalog of Compact Binary Mergers Observed by LIGO and Virgo during the First and Second Observing Runs, *Physical Review X* **9**, 031040 (2019), arXiv:1811.12907 [astro-ph.HE].
- [4] Abbott et al., GWTC-2: Compact Binary Coalescences Observed by LIGO and Virgo during the First Half of the Third Observing Run, *Physical Review X* **11**, 021053 (2021), arXiv:2010.14527 [gr-qc].
- [5] L. S. Collaboration, V. Collaboration, and K. Collaboration, Gwtc-3: Compact binary coalescences observed by ligo and virgo during the second part of the third observing run — data behind the figures (2023).
- [6] The LIGO Scientific Collaboration, the Virgo Collaboration, and the KAGRA Collaboration, GWTC-5.0: Observations from the Second Part of the Fourth LIGO-Virgo-KAGRA Observing Run and Updates to the Gravitational-Wave Transient Catalog, arXiv e-prints , arXiv:2605.27225 (2026), arXiv:2605.27225 [gr-qc].
- [7] The LIGO Scientific Collaboration, the Virgo Collaboration, and the KAGRA Collaboration, GWTC-5.0: Population Properties of Merging Compact Binaries, arXiv e-prints , arXiv:2605.27226 (2026), arXiv:2605.27226 [astro-ph.HE].
- [8] Abbott et al., Population Properties of Compact Objects from the Second LIGO-Virgo Gravitational-Wave Transient Catalog, *ApJL* **913**, L7 (2021), arXiv:2010.14533 [astro-ph.HE].
- [9] LIGO Scientific Collaboration and Virgo Collaboration, Binary Black Hole Population Properties Inferred from the First and Second Observing Runs of Advanced LIGO and Advanced Virgo, *ApJL* **882**, L24 (2019), arXiv:1811.12940 [astro-ph.HE].
- [10] Abbott et al., Population Properties of Compact Objects from the Second LIGO-Virgo Gravitational-Wave Transient Catalog, *ApJL* **913**, L7 (2021), arXiv:2010.14533 [astro-ph.HE].
- [11] R. Abbott, T. D. Abbott, F. Acernese, K. Ackley, C. Adams, N. Adhikari, R. X. Adhikari, V. B. Adya, C. Affeldt, D. Agarwal, M. Agathos, K. Agatsuma, N. Aggarwal, O. D. Aguiar, L. Aiello, A. Ain, P. Ajith, T. Akutsu, P. F. de Alarcón, S. Akcay, S. Albanesi, A. Allocca, P. A. Altin, A. Amato, C. Anand, S. Anand, A. Ananyeva, S. B. Anderson, W. G. Anderson, M. Ando, T. Andrade, N. Andres, T. Andrić, S. V. Angelova, S. Ansoldi, J. M. Antelis, S. Antier, F. Antonini, S. Appert, K. Arai, K. Arai, Y. Arai, S. Araki, A. Araya, M. C. Araya, J. S. Areeda, M. Arène, N. Aritomi, N. Arnaud, M. Arogeti, S. M. Aronson, K. G. Arun, H. Asada, Y. Asali, G. Ashton, Y. Aso, M. Assiduo, S. M. Aston, P. Astone, F. Aubin, C. Austin, S. Babak, F. Badaracco, M. K. M. Bader, C. Badger, S. Bae, Y. Bae, A. M. Baer, S. Bagnasco, Y. Bai, L. Baiotti, J. Baird, R. Bajpai, M. Ball, G. Ballardín, S. W. Ballmer, A. Balsamo, G. Baltus, S. Banagiri, D. Bankar, J. C. Barayoga, C. Barbieri, B. C. Barish, D. Barker, P. Barneo, F. Barone, B. Barr, L. Barsotti, M. Barsuglia, D. Barta, J. Bartlett, M. A. Barton, I. Bartos, R. Bassiri, A. Basti, M. Bawaj, J. C. Bayley, A. C. Baylor, M. Bazzan, B. Bécsy, V. M. Bedakihale, M. Bejger, I. Belahcene, V. Benedetto, D. Beniwal, T. F. Bennett, J. D. Bentley, M. Benyaala, F. Bergamin, B. K. Berger, S. Bernuzzi, C. P. L. Berry, D. Bersanetti, A. Bertolini, J. Betzwieser, D. Beveridge, R. Bhandare, U. Bhardwaj, D. Bhat-

- tacharjee, S. Bhaumik, I. A. Bilenko, G. Billingsley, S. Bini, R. Birney, O. Birnholtz, S. Biscans, M. Bisch, S. Biscoveanu, A. Bisht, B. Biswas, M. Bitossi, M. A. Bizouard, J. K. Blackburn, C. D. Blair, D. G. Blair, R. M. Blair, F. Bobba, N. Bode, M. Boer, G. Bogaert, M. Boldrini, L. D. Bonavena, F. Bondu, E. Bonilla, R. Bonnand, P. Booker, B. A. Boom, R. Bork, V. Boschi, N. Bose, S. Bose, V. Bossilkov, V. Boudart, Y. Bouffanais, A. Bozzi, C. Bradaschia, P. R. Brady, A. Bramley, A. Branch, M. Branchesi, J. Brandt, J. E. Brau, M. Breschi, T. Briant, J. H. Briggs, A. Brillet, M. Brinkmann, P. Brockill, A. F. Brooks, J. Brooks, D. D. Brown, S. Brunett, G. Bruno, R. Bruntz, J. Bryant, T. Bulik, H. J. Bulten, A. Buonanno, R. Busicchio, D. Buskulic, C. Buy, R. L. Byer, L. Cadonati, G. Cagnoli, C. Cahillane, J. C. Bustillo, J. D. Callaghan, T. A. Callister, E. Calloni, J. Cameron, J. B. Camp, M. Canepa, S. Canevarolo, M. Cannavacciuolo, K. C. Cannon, H. Cao, Z. Cao, E. Capocasa, E. Capote, and G. Carapella, Population of Merging Compact Binaries Inferred Using Gravitational Waves through GWTC-3, *Physical Review X* **13**, 011048 (2023), arXiv:2111.03634 [astro-ph.HE].
- [12] J. Godfrey, B. Edelman, and B. Farr, Cosmic Cousins: Identification of a Subpopulation of Binary Black Holes Consistent with Isolated Binary Evolution, arXiv e-prints, arXiv:2304.01288 (2023), arXiv:2304.01288 [astro-ph.HE].
- [13] J. Sadiq, T. Dent, and A. Lorenzo-Medina, Seeking Spinning Subpopulations of Black Hole Binaries via Iterative Density Estimation, arXiv e-prints, arXiv:2506.02250 (2025), arXiv:2506.02250 [astro-ph.HE].
- [14] Y.-Z. Wang, Y.-J. Li, J. S. Vink, Y.-Z. Fan, S.-P. Tang, Y. Qin, and D.-M. Wei, Potential Subpopulations and Assembling Tendency of the Merging Black Holes, *ApJL* **941**, L39 (2022), arXiv:2208.11871 [astro-ph.HE].
- [15] S. Biscoveanu, T. A. Callister, C.-J. Haster, K. K. Y. Ng, S. Vitale, and W. M. Farr, The Binary Black Hole Spin Distribution Likely Broadens with Redshift, *ApJL* **932**, L19 (2022), arXiv:2204.01578 [astro-ph.HE].
- [16] T. A. Callister, C.-J. Haster, K. K. Y. Ng, S. Vitale, and W. M. Farr, Who Ordered That? Unequal-mass Binary Black Hole Mergers Have Larger Effective Spins, *ApJL* **922**, L5 (2021), arXiv:2106.00521 [astro-ph.HE].
- [17] F. Antonini, M. Gieles, F. Dosopoulou, and D. Chattopadhyay, Coalescing black hole binaries from globular clusters: mass distributions and comparison to gravitational wave data from GWTC-3, *MNRAS* **522**, 466 (2023), arXiv:2208.01081 [astro-ph.HE].
- [18] A. Hussain, M. Isi, and A. Zimmerman, Hints of spin-magnitude correlations and a rapidly spinning subpopulation of binary black holes (2024), arXiv:2411.02252 [astro-ph.HE].
- [19] A. Ray, I. M. Hernandez, K. Breivik, and J. Creighton, Searching for binary black hole sub-populations in gravitational wave data using binned gaussian processes (2024), arXiv:2404.03166 [astro-ph.HE].
- [20] S. Banagiri, E. Thrane, and P. D. Lasky, Evidence for three subpopulations of merging binary black holes at different primary masses (2025), arXiv:2509.15646 [astro-ph.HE].
- [21] S. Padhyegurjar and S. Mukherjee, The first detection of sub-populations in the delay-time distribution of binary black holes in gwtc-4 of ligo-virgo-kagra (2026), arXiv:2606.02318 [astro-ph.HE].
- [22] F. Antonini, I. Romero-Shaw, and T. Callister, Gravitational-wave constraints on the pair-instability mass gap and nuclear burning in massive stars, *Nat Astron* **10**.1038/s41550-026-02847-0.
- [23] H. Tong, M. Fishbach, and E. Thrane, Evidence of the pair-instability gap from black-hole masses, *Nature* **652**, 874–877.
- [24] U. N. Di Carlo, M. Mapelli, Y. Bouffanais, N. Giacobbo, F. Santoliquido, A. Bressan, M. Spera, and F. Haardt, Binary black holes in the pair instability mass gap, *MNRAS* **497**, 1043 (2020), arXiv:1911.01434 [astro-ph.HE].
- [25] C. Hoy, S. Fairhurst, M. Hannam, and V. Tiwari, Understanding How Fast Black Holes Spin by Analyzing Data from the Second Gravitational-wave Catalogue, *ApJ* **928**, 75 (2022), arXiv:2110.13542 [gr-qc].
- [26] F. Antonini, I. M. Romero-Shaw, and T. Callister, Star Cluster Population of High Mass Black Hole Mergers in Gravitational Wave Data, *Phys. Rev. Lett.* **134**, 011401 (2025), arXiv:2406.19044 [astro-ph.HE].
- [27] I. Magaña Hernandez and A. Palmese, Astrophysics informed Gaussian processes for gravitational-wave populations: Evidence for the onset of the pair-instability supernova mass gap, arXiv e-prints, arXiv:2508.19208 (2025), arXiv:2508.19208 [astro-ph.HE].
- [28] C. Karathanasis, S. Mukherjee, and S. Mastrogiovanni, Binary black holes population and cosmology in new lights: signature of PISN mass and formation channel in GWTC-3, *MNRAS* **523**, 4539 (2023), arXiv:2204.13495 [astro-ph.CO].
- [29] S. Afroz and S. Mukherjee, Phase space of binary black holes from gravitational wave observations to unveil its formation history (2025), arXiv:2411.07304 [astro-ph.HE].
- [30] S. Afroz and S. Mukherjee, Binary black hole phase space discovers the signature of pair instability supernovae mass gap (2025), arXiv:2509.09123 [astro-ph.HE].
- [31] S. Padhyegurjar and S. Mukherjee, Bbh-genesis: Distinguishing binary black hole formation channels with gwtc-4 (2026), arXiv:2606.00234 [astro-ph.HE].
- [32] S. Biscoveanu, The first decade of gravitational-wave measurements of black hole spins (2026), arXiv:2606.06209 [gr-qc].
- [33] É. Racine, Analysis of spin precession in binary black hole systems including quadrupole-monopole interaction, *Phys. Rev. D* **78**, 044021 (2008), arXiv:0803.1820 [gr-qc].
- [34] W. M. Farr, S. Stevenson, M. C. Miller, I. Mandel, B. Farr, and A. Vecchio, Distinguishing spin-aligned and isotropic black hole populations with gravitational waves, *Nature* **548**, 426 (2017).
- [35] P. Hut, Tidal evolution in close binary systems., *A&A* **99**, 126 (1981).
- [36] D. Gerosa, E. Berti, R. O’Shaughnessy, K. Belczynski, M. Kesden, D. Wysocki, and W. Gladysz, Spin orientations of merging black holes formed from the evolution of stellar binaries, *Physical Review D* **98**, 10.1103/physrevd.98.084036 (2018).
- [37] C. L. Rodriguez, M. Zevin, C. Pankow, V. Kalogera, and F. A. Rasio, Illuminating Black Hole Binary Formation Channels with Spins in Advanced LIGO, *ApJL*, In Press 10.3847/2041-8205/832/1/L2 (2016).

- [38] P. Marchant, N. Langer, P. Podsiadlowski, T. M. Tauris, and T. J. Moriya, *Astronomy & Astrophysics A new route towards merging massive black holes*, *A&A* **588**, 10.1051/0004-6361/201628133 (2016).
- [39] S. E. de Mink and I. Mandel, *The chemically homogeneous evolutionary channel for binary black hole mergers: rates and properties of gravitational-wave events detectable by advanced LIGO*, *MNRAS* **460**, 3545 (2016), arXiv:1603.02291 [astro-ph.HE].
- [40] C. Adamcewicz, P. D. Lasky, and E. Thrane, *Evidence for a Correlation between Binary Black Hole Mass Ratio and Black Hole Spins*, *ApJ* **958**, 13 (2023), arXiv:2307.15278 [astro-ph.HE].
- [41] R. M. O’Leary, F. A. Rasio, J. M. Fregeau, N. Ivanova, and R. O’Shaughnessy, *Binary Mergers and Growth of Black Holes in Dense Star Clusters*, *The Astrophysical Journal* **637**, 937 (2006).
- [42] M. Fishbach, C. Kimball, and V. Kalogera, *Limits on Hierarchical Black Hole Mergers from the Most Negative χ_{eff} Systems*, *ApJL* **935**, L26 (2022), arXiv:2207.02924 [astro-ph.HE].
- [43] C. L. Rodriguez, M. Morscher, B. Pattabiraman, S. Chatterjee, C.-J. Haster, and F. A. Rasio, *Binary Black Hole Mergers from Globular Clusters: Implications for Advanced LIGO*, *Physical Review Letters* **115**, 051101 (2015).
- [44] Y. B. Ginat, F. Antonini, E. Flanagan, and M. Gieles, *Second-generation mass peak in the gravitational-wave population as a probe of globular clusters* (2026), arXiv:2604.07456 [astro-ph.HE].
- [45] C. Kimball, C. Talbot, C. P. L. Berry, M. Carney, M. Zevin, E. Thrane, and V. Kalogera, *Black Hole Genealogy: Identifying Hierarchical Mergers with Gravitational Waves*, *ApJ* **900**, 177 (2020), arXiv:2005.00023 [astro-ph.HE].
- [46] P. G. Breen and D. C. Heggie, *Dynamical evolution of black hole subsystems in idealized star clusters*, *Monthly Notices of the Royal Astronomical Society* **432**, 2779 (2013).
- [47] S. Torniamenti, M. Mapelli, C. Périgois, M. Arca Sedda, M. C. Artale, M. Dall’Amico, and M. P. Vaccaro, *Hierarchical binary black hole mergers in globular clusters: mass function and evolution with redshift*, arXiv e-prints , arXiv:2401.14837 (2024), arXiv:2401.14837 [astro-ph.HE].
- [48] K. Silsbee and S. Tremaine, *Lidov–Kozai Cycles with Gravitational Radiation: Merging Black Holes in Isolated Triple Systems*, *The Astrophysical Journal* **836**, 39 (2017).
- [49] F. Antonini, S. Toonen, and A. S. Hamers, *Binary Black Hole Mergers from Field Triples: Properties, Rates, and the Impact of Stellar Evolution*, *ApJ* **841**, 77 (2017), arXiv:1703.06614 [astro-ph.GA].
- [50] B. Liu and D. Lai, *Hierarchical black hole mergers in multiple systems: constrain the formation of GW190412-, GW190814-, and GW190521-like events*, *MNRAS* **502**, 2049 (2021), arXiv:2009.10068 [astro-ph.HE].
- [51] G. Fragione and B. Kocsis, *Black hole mergers from quadruples*, *MNRAS* **486**, 4781 (2019), arXiv:1903.03112 [astro-ph.GA].
- [52] J. Stegmann, F. Antonini, F. R. N. Schneider, V. Tiwari, and D. Chattopadhyay, *Binary black hole mergers from merged stars in the Galactic field*, arXiv e-prints , arXiv:2203.16544 (2022), arXiv:2203.16544 [astro-ph.GA].
- [53] M. A. S. Martinez, C. L. Rodriguez, and G. Fragione, *On the Mass Ratio Distribution of Black Hole Mergers in Triple Systems*, *ApJ* **937**, 78 (2022), arXiv:2105.01671 [astro-ph.SR].
- [54] B. McKernan and K. E. S. Ford, *Constraining the LVK AGN channel with black hole spins*, *MNRAS* **531**, 3479 (2024), arXiv:2309.15213 [astro-ph.HE].
- [55] I. Bartos, B. Kocsis, Z. Haiman, and S. Márka, *Rapid and Bright Stellar-mass Binary Black Hole Mergers in Active Galactic Nuclei*, *ApJ* **835**, 165 (2017), arXiv:1602.03831 [astro-ph.HE].
- [56] H. Tagawa, B. Kocsis, Z. Haiman, I. Bartos, K. Omukai, and J. Samsing, *Mass-gap Mergers in Active Galactic Nuclei*, *ApJ* **908**, 194 (2021), arXiv:2012.00011 [astro-ph.HE].
- [57] Y. Yang, I. Bartos, V. Gayathri, K. E. S. Ford, Z. Haiman, S. Klimentko, B. Kocsis, S. Márka, Z. Márka, B. McKernan, and R. O’Shaughnessy, *Hierarchical Black Hole Mergers in Active Galactic Nuclei*, *Phys. Rev. Lett.* **123**, 181101 (2019), arXiv:1906.09281 [astro-ph.HE].
- [58] S. Bird, I. Cholis, J. B. Muñoz, Y. Ali-Haïmoud, M. Kamionkowski, E. D. Kovetz, A. Raccanelli, and A. G. Riess, *Did LIGO Detect Dark Matter?*, *Phys. Rev. Lett.* **116**, 201301 (2016), arXiv:1603.00464 [astro-ph.CO].
- [59] M. Sasaki, T. Suyama, T. Tanaka, and S. Yokoyama, *Primordial Black Hole Scenario for the Gravitational-Wave Event GW150914*, *Phys. Rev. Lett.* **117**, 061101 (2016), arXiv:1603.08338 [astro-ph.CO].
- [60] V. De Luca, G. Franciolini, P. Pani, and A. Riotto, *The evolution of primordial black holes and their final observable spins*, *J. Cosmology Astropart. Phys.* **2020**, 052 (2020), arXiv:2003.02778 [astro-ph.CO].
- [61] G. Franciolini, V. Baibhav, V. De Luca, K. K. Y. Ng, K. W. K. Wong, E. Berti, P. Pani, A. Riotto, and S. Vitale, *Searching for a subpopulation of primordial black holes in LIGO-Virgo gravitational-wave data*, *Phys. Rev. D* **105**, 083526 (2022), arXiv:2105.03349 [gr-qc].
- [62] V. De Luca, G. Franciolini, and A. Riotto, *GW231123: a Possible Primordial Black Hole Origin*, arXiv e-prints , arXiv:2508.09965 (2025), arXiv:2508.09965 [astro-ph.CO].
- [63] M. Safarzadeh, W. M. Farr, and E. Ramirez-Ruiz, *A Trend in the Effective Spin Distribution of LIGO Binary Black Holes with Mass*, *ApJ* **894**, 129 (2020), arXiv:2001.06490 [gr-qc].
- [64] K. Belczynski, J. Klencki, C. E. Fields, A. Olejak, E. Berti, G. Meynet, C. L. Fryer, D. E. Holz, R. O’Shaughnessy, D. A. Brown, T. Bulik, S. C. Leung, K. Nomoto, P. Madau, R. Hirschi, E. Kaiser, S. Jones, S. Mondal, M. Chruslinska, P. Drozda, D. Gerosa, Z. Doctor, M. Giersz, S. Ekstrom, C. Georgy, A. Askar, V. Baibhav, D. Wysocki, T. Natan, W. M. Farr, G. Wiktorowicz, M. Coleman Miller, B. Farr, and J.-P. Lasota, *Evolutionary roads leading to low effective spins, high black hole masses, and O1/O2 rates for LIGO/Virgo binary black holes*, *A&A* **636**, A104 (2020), arXiv:1706.07053 [astro-ph.HE].
- [65] G. Pierra, S. Mastrogiovanni, and S. Perriès, *The spin magnitude of stellar-mass binary black holes*

- evolves with the mass: evidence from gravitational wave data, arXiv e-prints , arXiv:2406.01679 (2024), arXiv:2406.01679 [gr-qc].
- [66] H. Tong, T. A. Callister, M. Fishbach, E. Thrane, F. Antonini, S. Stevenson, I. M. Romero-Shaw, and F. Dosopoulou, A subpopulation of low-mass, spinning black holes: signatures of dynamical assembly, arXiv e-prints , arXiv:2511.05316 (2025), arXiv:2511.05316 [astro-ph.HE].
- [67] J. Heinzl, M. Mould, and S. Vitale, Nonparametric analysis of correlations in the binary black hole population with LIGO-Virgo-KAGRA data, Phys. Rev. D **111**, L061305 (2025), arXiv:2406.16844 [astro-ph.HE].
- [68] F. Antonini, T. Callister, F. Dosopoulou, I. Romero-Shaw, and D. Chattopadhyay, Inferring the pair-instability mass gap from gravitational wave data using flexible models, arXiv e-prints , arXiv:2506.09154 (2025), arXiv:2506.09154 [astro-ph.HE].
- [69] J. Sadiq, T. Dent, and A. Lorenzo-Medina, Seeking Spinning Subpopulations of Black Hole Binaries via Iterative Density Estimation, arXiv e-prints , arXiv:2506.02250 (2025), arXiv:2506.02250 [astro-ph.HE].
- [70] S. Banagiri, E. Thrane, and P. D. Lasky, Evidence for Three Subpopulations of Merging Binary Black Holes at Different Primary Masses, arXiv e-prints , arXiv:2509.15646 (2025), arXiv:2509.15646 [astro-ph.HE].
- [71] A. Ray, S. Mukherjee, M. Zevin, and V. Kalogera, On the Astrophysical Origin of Binary Black Hole Subpopulations: A Tale of Three Channels?, arXiv e-prints , arXiv:2603.17987 (2026), arXiv:2603.17987 [astro-ph.HE].
- [72] M. Mould, J. Heinzl, S. Álvarez-López, C. Plunkett, N. E. Wolfe, and S. Vitale, Measurement prospects for the pair-instability mass cutoff with gravitational waves, Phys. Rev. D **113**, 103021 (2026), arXiv:2602.11282 [astro-ph.HE].
- [73] C. Plunkett, T. Callister, M. Zevin, and S. Vitale, Signatures of a subpopulation of hierarchical mergers in the gwtc-4 gravitational-wave dataset (2026), arXiv:2601.07908 [gr-qc].
- [74] Y.-Z. Wang, Y.-J. Li, J. S. Vink, Y.-Z. Fan, S.-P. Tang, Y. Qin, and D.-M. Wei, Potential Subpopulations and Assembling Tendency of the Merging Black Holes, Astrophys. J. Lett. **941**, L39 (2022), arXiv:2208.11871 [astro-ph.HE].
- [75] Y.-J. Li, Y.-Z. Wang, S.-P. Tang, and Y.-Z. Fan, Resolving the Stellar-Collapse and Hierarchical-Merger Origins of the Coalescing Black Holes, Phys. Rev. Lett. **133**, 051401 (2024), arXiv:2303.02973 [astro-ph.HE].
- [76] C. Kimball, C. Talbot, C. P. L. Berry, M. Zevin, E. Thrane, V. Kalogera, R. Busicchio, M. Carney, T. Dent, H. Middleton, E. Payne, J. Veitch, and D. Williams, Evidence for Hierarchical Black Hole Mergers in the Second LIGO-Virgo Gravitational Wave Catalog, ApJL **915**, L35 (2021), arXiv:2011.05332 [astro-ph.HE].
- [77] J. Golomb and C. Talbot, Searching for structure in the binary black hole spin distribution, Phys. Rev. D **108**, 103009 (2023), arXiv:2210.12287 [astro-ph.HE].
- [78] L. S. Collaboration, V. Collaboration, and K. Collaboration, Gwtc-4: Compact binary coalescences observed by ligo and virgo during the o3b observing run (2025).
- [79] V. Baibhav, D. Gerosa, E. Berti, K. W. K. Wong, T. Helfer, and M. Mould, The mass gap, the spin gap, and the origin of merging binary black holes, Phys. Rev. D **102**, 043002 (2020), arXiv:2004.00650 [astro-ph.HE].
- [80] J. Sadiq, T. Dent, and M. Gieles, Binary Vision: The Mass Distribution of Merging Binary Black Holes via Iterative Density Estimation, ApJ **960**, 65 (2024), arXiv:2307.12092 [astro-ph.HE].
- [81] e. a. Abbott, R., Open data from the third observing run of ligo, virgo, kagra, and geo, The Astrophysical Journal Supplement Series **267**, 29 (2023).
- [82] T. L. S. Collaboration, the Virgo Collaboration, the KAGRA Collaboration, and e. a. A. G. Abac, Open data from ligo, virgo, and kagra through the first part of the fourth observing run (2025), arXiv:2508.18079 [gr-qc].
- [83] e. a. Abbott, R., Open data from the first and second observing runs of advanced ligo and advanced virgo, SoftwareX **13**, 100658 (2021).
- [84] A. Buikema, C. Cahillane, G. L. Mansell, *et al.*, Sensitivity and performance of the Advanced LIGO detectors in the third observing run, Phys. Rev. D **102**, 062003 (2020), arXiv:2008.01301 [astro-ph.IM].
- [85] e. a. Abbott, B.P., Prospects for observing and localizing gravitational-wave transients with Advanced LIGO, Advanced Virgo and KAGRA, Living Reviews in Relativity **23**, 3 (2020).
- [86] e. a. Tse, M., Quantum-Enhanced Advanced LIGO Detectors in the Era of Gravitational-Wave Astronomy, Phys. Rev. Lett. **123**, 231107 (2019).
- [87] e. a. Martynov, D.V., Sensitivity of the Advanced LIGO detectors at the beginning of gravitational wave astronomy, Phys. Rev. D **93**, 112004 (2016), arXiv:1604.00439 [astro-ph.IM].
- [88] Virgo Collaboration, Advanced Virgo: a second-generation interferometric gravitational wave detector, Classical and Quantum Gravity **32**, 024001 (2015), arXiv:1408.3978 [gr-qc].
- [89] LIGO Scientific Collaboration and e. a. Aasi, J., Advanced LIGO, Classical and Quantum Gravity **32**, 074001 (2015), arXiv:1411.4547 [gr-qc].
- [90] e. a. Akutsu, T., Overview of KAGRA: Detector design and construction history, Progress of Theoretical and Experimental Physics **2021**, 05A101 (2021), arXiv:2005.05574 [physics.ins-det].
- [91] R. e. a. Abbott (LIGO Scientific Collaboration, Virgo Collaboration, and KAGRA Collaboration), Gwtc-3: Compact binary coalescences observed by ligo and virgo during the second part of the third observing run, Phys. Rev. X **13**, 041039 (2023).
- [92] R. Essick, M. W. Coughlin, M. Zevin, D. Chatterjee, T. A. Clarke, S. Colloms, U. Mali, S. Miller, N. Steinle, P. Baral, A. C. Baylor, G. Cabourn Davies, T. Dent, P. Joshi, P. Kumar, C. Messick, T. Mishra, A. Ouzriat, K. S. Phukon, L. Piccari, M. Pillas, M. Trevor, T. A. Callister, and M. Fishbach, Compact binary coalescence sensitivity estimates with injection campaigns during the ligo-virgo-kagra collaborations' fourth observing run, Phys. Rev. D **112**, 102001 (2025).
- [93] H. Tong, T. A. Callister, M. Fishbach, E. Thrane, F. Antonini, S. Stevenson, I. M. Romero-Shaw, and F. Dosopoulou, A subpopulation of low-mass, spinning black holes: signatures of dynamical assembly (2025),

- arXiv:2511.05316 [astro-ph.HE].
- [94] R. e. a. Abbott, Gwtc-2: Compact binary coalescences observed by ligo and virgo during the first half of the third observing run, *Physical Review X* **11**, 10.1103/physrevx.11.021053 (2021).
- [95] The LIGO Scientific Collaboration, the Virgo Collaboration, and the KAGRA Collaboration, GWTC-4.0: Population Properties of Merging Compact Binaries, arXiv e-prints , arXiv:2508.18083 (2025), arXiv:2508.18083 [astro-ph.HE].
- [96] A. G. Abac, I. Abouelfettouh, F. Acernese, K. Ackley, C. Adamcewicz, S. Adhichary, D. Adhikari, N. Adhikari, R. X. Adhikari, V. K. Adkins, S. Afroz, A. Agapito, D. Agarwal, M. Agathos, N. Aggarwal, S. Aggarwal, O. D. Aguiar, I.-L. Ahrend, L. Aiello, A. Ain, P. Ajith, T. Akutsu, S. Albanesi, W. Ali, S. Al-Kersh, C. All  n  , A. Allocca, S. Al-Shammari, P. A. Altin, S. Alvarez-Lopez, W. Amar, O. Amarasinghe, A. Amato, F. Amicucci, C. Amra, A. Ananyeva, S. B. Anderson, W. G. Anderson, M. Andia, M. Ando, M. Andr  s-Carcasona, T. Andri  , J. Anglin, S. Ansoldi, J. M. Antelis, S. Antier, F. Antonini, M. Aoumi, E. Z. Appavuvavther, S. Appert, S. K. Apple, K. Arai, C. Ara  jo-  lvarez, A. Araya, M. C. Araya, M. A. Sedda, J. S. Areeda, N. Aritomi, F. Armato, S. Armstrong, N. Arnaud, M. Arogeti, S. M. Aronson, K. G. Arun, G. Ashton, Y. Aso, L. Asprea, M. Assiduo, S. Assis de Souza Melo, S. M. Aston, P. Astone, P. S. Aswathi, F. Atadiao, F. Aubin, K. Aultoneal, G. Avallone, E. A. Avila, S. Babak, C. Badger, S. Bae, S. Bagnasco, L. Baiotti, R. Bajpai, T. Baka, A. M. Baker, K. A. Baker, T. Baker, G. Baldi, N. Baldicchi, M. Ball, G. Ballardin, S. W. Ballmer, S. Banagiri, B. Banerjee, D. Bankar, T. M. Baptiste, P. Baral, M. Baratti, J. C. Barayoga, B. C. Barish, D. Barker, N. Barman, P. Barneo, F. Barone, B. Barr, L. Barsotti, M. Barsuglia, D. Barta, A. M. Bartoletti, M. A. Barton, I. Bartos, A. Basalae, R. Bassiri, A. Basti, M. Bawaj, P. Baxi, J. C. Bayley, A. C. Baylor, P. A. Baynard, II, M. Bazzan, V. M. Bedakihale, F. Beirnaert, M. Berger, D. Belardinelli, A. S. Bell, D. S. Bellie, L. Bellizzi, W. Benoit, I. Bentara, J. D. Bentley, M. Ben Yaala, S. Bera, F. Bergamin, B. K. Berger, S. Bernuzzi, M. Beroiz, C. P. L. Berry, D. Bersanetti, T. Bertheas, A. Bertolini, J. Betzwieser, D. Beveridge, G. Bevilacqua, N. Bevins, R. Bhandare, R. Bhatt, D. Bhattacharjee, S. Bhattacharyya, S. Bhaumik, V. Biancalana, A. Bianchi, I. A. Bilenko, G. Billingsley, A. Binetti, S. Bini, C. Binu, S. Biot, O. Birnholtz, S. Biscoveanu, A. Bisht, M. Bitossi, M.-A. Bizouard, S. Blaber, J. K. Blackburn, L. A. Blagg, C. D. Blair, D. G. Blair, N. Bode, N. Boettner, G. Boileau, M. Boldrini, G. N. Bolingbroke, A. Bolliand, L. D. Bonavena, R. Bondarescu, F. Bondu, E. Bonilla, M. S. Bonilla, A. Bonino, R. Bonnand, A. Borchers, S. Borhanian, V. Boschi, S. Bose, V. Bossilkov, Y. Bothra, A. Boudon, L. Bour, M. Boyle, A. Bozzi, C. Bradaschia, P. R. Brady, A. Branch, M. Branchesi, I. Braun, T. Briant, A. Brillet, M. Brinkmann, P. Brockill, and E. Brockmueller, GW241011 and GW241110: Exploring Binary Formation and Fundamental Physics with Asymmetric, High-spin Black Hole Coalescences, *ApJL* **993**, L21 (2025), arXiv:2510.26931 [astro-ph.HE].
- [97] S. Galaudage and A. Lamberts, Compactness peaks: An astrophysical interpretation of the mass distribution of merging binary black holes, *Astronomy & Astrophysics* **694**, A186 (2025).
- [98] O. Sridhar, A. Ray, and V. Kalogera, Characterizing binary black hole subpopulations in gwtc-4 with binned gaussian processes: On the origins of the $35m_{\odot}$ peak (2025), arXiv:2511.22093 [astro-ph.HE].
- [99] Y.-J. Li, Y.-Z. Wang, S.-P. Tang, Q. Yuan, Y.-Z. Fan, and D.-M. Wei, Divergence in mass ratio distributions between low-mass and high-mass coalescing binary black holes, *The Astrophysical Journal Letters* **933**, L14 (2022).
- [100] Y.-J. Li, S.-P. Tang, S.-J. Gao, D.-C. Wu, and Y.-Z. Wang, Exploring field-evolution and dynamical-capture coalescing binary black holes in gwtc-3, *The Astrophysical Journal* **977**, 67 (2024).
- [101] S. Kishore Roy, L. A. C. van Son, and W. M. Farr, A mid-thirties crisis: dissecting the properties of gravitational wave sources near the 35 solar mass peak, *Classical and Quantum Gravity* **42**, 225008 (2025).
- [102] A. Ray, S. Mukherjee, M. Zevin, and V. Kalogera, On the astrophysical origin of binary black hole subpopulations: A tale of three channels? (2026), arXiv:2603.17987 [astro-ph.HE].
- [103] A. M. Farah, A. Vijaykumar, and M. Fishbach, The Steep Redshift Evolution of the Hierarchical Binary Black Hole Merger Rate May Cause the z - χ_{eff} Correlation, *Astrophys. J. Lett.* **1001**, L40 (2026), arXiv:2601.03456 [astro-ph.HE].
- [104] A. Vijaykumar, A. M. Farah, and M. Fishbach, The Maximum Mass Ratio of Hierarchical Binary Black Hole Mergers May Cause the q - χ_{eff} Correlation, *Astrophys. J. Lett.* **999**, L30 (2026), arXiv:2601.03457 [astro-ph.HE].
- [105] S. Banagiri, T. A. Callister, C. Adamcewicz, Z. Doctor, and V. Kalogera, Structure and Skewness of the Effective Inspiral Spin Distribution of Binary Black Hole Mergers, *ApJ* **990**, 147 (2025), arXiv:2501.06712 [astro-ph.HE].
- [106] S. Alvarez-Lopez, J. Heinzl, and S. Vitale, Evidence for additional structure in the effective spin distribution hints at multiple formation pathways in gwtc-5.0 (2026), arXiv:2606.12205 [astro-ph.HE].
- [107] M. V. van der Sluys, C. R  ver, A. Stroeer, V. Raymond, I. Mandel, N. Christensen, V. Kalogera, R. Meyer, and A. Vecchio, Gravitational-wave astronomy with inspiral signals of spinning compact-object binaries, *Astrophys. J. Lett.* **688**, L61 (2008), arXiv:0710.1897 [astro-ph].
- [108] S. Vitale, R. Lynch, J. Veitch, V. Raymond, and R. Sturani, Measuring the Spin of Black Holes in Binary Systems Using Gravitational Waves, *Phys. Rev. Lett.* **112**, 251101 (2014), arXiv:1403.0129 [gr-qc].
- [109] S. Vitale, D. Gerosa, C.-J. Haster, K. Chatziioannou, and A. Zimmerman, Impact of Bayesian Priors on the Characterization of Binary Black Hole Coalescences, *Phys. Rev. Lett.* **119**, 251103 (2017), arXiv:1707.04637 [gr-qc].
- [110] A. Ghosh, W. Del Pozzo, and P. Ajith, Estimating parameters of binary black holes from gravitational-wave observations of their inspiral, merger and ringdown, *Phys. Rev. D* **94**, 104070 (2016), arXiv:1505.05607 [gr-qc].
- [111] K. Chatziioannou, G. Lovelace, M. Boyle, M. Giesler, D. A. Hemberger, R. Katebi, L. E. Kidder, H. P. Pfeiffer,

- M. A. Scheel, and B. Szilágyi, Measuring the properties of nearly extremal black holes with gravitational waves, *Phys. Rev. D* **98**, 044028 (2018), arXiv:1804.03704 [gr-qc].
- [112] G. Pratten, P. Schmidt, R. Buscicchio, and L. M. Thomas, Measuring precession in asymmetric compact binaries, *Phys. Rev. Research* **2**, 043096 (2020), arXiv:2006.16153 [gr-qc].
- [113] S. Biscoveanu, M. Isi, S. Vitale, and V. Varma, A New Spin on LIGO-Virgo Binary Black Holes, *Phys. Rev. Lett.* **126**, 171103 (2021), arXiv:2007.09156 [astro-ph.HE].
- [114] C. Cutler and É. E. Flanagan, Gravitational waves from merging compact binaries: How accurately can one extract the binary's parameters from the inspiral waveform?, *Phys. Rev. D* **49**, 2658 (1994), arXiv:gr-qc/9402014.
- [115] E. Poisson and C. M. Will, Gravitational waves from inspiraling compact binaries: Parameter estimation using second-post-Newtonian waveforms, *Phys. Rev. D* **52**, 848 (1995), arXiv:gr-qc/9502040.
- [116] E. Baird, S. Fairhurst, M. Hannam, and P. Murphy, Degeneracy between mass and spin in black-hole-binary waveforms, *Phys. Rev. D* **87**, 024035 (2013), arXiv:1211.0546 [gr-qc].
- [117] M. Pürrer, M. Hannam, P. Ajith, and S. Husa, Testing the validity of the single-spin approximation in inspiral-merger-ringdown waveforms, *Phys. Rev. D* **88**, 064007 (2013), arXiv:1306.2320 [gr-qc].
- [118] K. K. Y. Ng, S. Vitale, A. Zimmerman, K. Chatziioannou, D. Gerosa, and C.-J. Haster, Gravitational-wave astrophysics with effective-spin measurements: Asymmetries and selection biases, *Phys. Rev. D* **98**, 083007 (2018), arXiv:1805.03046 [gr-qc].
- [119] É. E. Flanagan and S. A. Hughes, Measuring gravitational waves from binary black hole coalescences. I. Signal to noise for inspiral, merger, and ringdown, *Phys. Rev. D* **57**, 4535 (1998), arXiv:gr-qc/9701039.
- [120] M. Campanelli, C. O. Lousto, and Y. Zlochower, Spinning-black-hole binaries: The orbital hang-up, *Phys. Rev. D* **74**, 041501 (2006), arXiv:gr-qc/0604012.
- [121] H. Tong, M. Fishbach, and E. Thrane, Spinning spectral sirens: Robust cosmological measurement using mass-spin correlations in the binary black hole population, arXiv e-prints, arXiv:2502.10780 (2025), arXiv:2502.10780 [astro-ph.CO].
- [122] Y. Qin and T. Fragos, The spin of the second-born black hole in coalescing binary black holes, *ApJ* **865**, 15 (2018).
- [123] S. S. Bavera, M. Zevin, T. Fragos, *et al.*, The impact of black hole natal kicks on spin-orbit misalignment in merging binary black holes, *A&A* **635**, A97 (2020).
- [124] J. Fuller and L. Ma, Most Black Holes Are Born Very Slowly Rotating, *ApJL* **881**, L1 (2019), arXiv:1907.03714 [astro-ph.SR].
- [125] K. Belczynski, R. Hirschi, E. Kaiser, *et al.*, The formation and gravitational-wave detection of massive stellar black hole binaries, *A&A* **636**, A104 (2020).
- [126] K. Belczynski, V. Kalogera, F. A. Rasio, R. E. Taam, A. Zezas, T. Bulik, T. J. Maccarone, and N. Ivanova, Compact Object Modeling with the StarTrack Population Synthesis Code, *The Astrophysical Journal Supplement Series* **174**, 223 (2008).
- [127] M. Dominik, K. Belczynski, C. Fryer, *et al.*, Double compact objects. i. the significance of the common envelope on merger rates, *ApJ* **759**, 52 (2012).
- [128] S. E. de Mink and I. Mandel, The chemically homogeneous evolutionary channel for binary black hole mergers, *MNRAS* **460**, 3545 (2016).
- [129] A. Olejak and K. Belczynski, The Implications of High Black Hole Spins for the Origin of Binary Black Hole Mergers, *ApJL* **921**, L2 (2021), arXiv:2109.06872 [astro-ph.HE].
- [130] J. Stegmann, F. Antonini, F. R. N. Schneider, V. Tiwari, and D. Chattopadhyay, Binary black hole mergers from merged stars in the Galactic field, *Phys. Rev. D* **106**, 023014 (2022), arXiv:2203.16544 [astro-ph.GA].
- [131] F. Antonini, C. L. Rodriguez, C. Petrovich, and C. L. Fischer, Precessional dynamics of black hole triples: binary mergers with near-zero effective spin, *MNRAS* **480**, L58 (2018), arXiv:1711.07142 [astro-ph.HE].
- [132] J. Stegmann, F. Antonini, A. Olejak, S. Biscoveanu, V. Raymond, S. Rinaldi, and E. Flanagan, Gravitational-wave Observations Suggest Most Black Hole Mergers Form in Triples, *ApJL* **1000**, L59 (2026), arXiv:2512.15873 [astro-ph.HE].
- [133] Y.-H. Wang, B. McKernan, S. Ford, R. Perna, N. W. C. Leigh, and M.-M. Mac Low, Symmetry Breaking in Dynamical Encounters in the Disks of Active Galactic Nuclei, *ApJL* **923**, L23 (2021), arXiv:2110.03698 [astro-ph.HE].
- [134] M. Arca Sedda, M. Mapelli, M. Benacquista, and M. Spera, Isolated and dynamical black hole mergers with B-POP: the role of star formation and dynamics, star cluster evolution, natal kicks, mass and spins, and hierarchical mergers, *MNRAS* **520**, 5259 (2023), arXiv:2109.12119 [astro-ph.GA].
- [135] F. Antonini, M. Gieles, F. Dosopoulou, and D. Chattopadhyay, Coalescing black hole binaries from globular clusters: mass distributions and comparison to gravitational wave data from GWTC-3, *MNRAS* **522**, 466 (2023), arXiv:2208.01081 [astro-ph.HE].
- [136] D. Chattopadhyay, J. Hurley, S. Stevenson, and A. Raidani, Dynamical double black holes and their host cluster properties, *MNRAS* **513**, 4527 (2022), arXiv:2202.08924 [astro-ph.GA].
- [137] M. Spera and M. Mapelli, Very massive stars, pair-instability supernovae and intermediate-mass black holes with the sevn code, *MNRAS* **470**, 4739 (2017), arXiv:1706.06109 [astro-ph.SR].
- [138] R. Farmer, M. Renzo, S. E. de Mink, P. Marchant, and S. Justham, Mind the Gap: The Location of the Lower Edge of the Pair-instability Supernova Black Hole Mass Gap, *ApJ* **887**, 53 (2019), arXiv:1910.12874 [astro-ph.SR].
- [139] M. Renzo, E. Zapartas, S. E. de Mink, Y. Götberg, S. Justham, R. J. Farmer, R. G. Izzard, S. Toonen, and H. Sana, Massive runaway and walkaway stars. A study of the kinematical imprints of the physical processes governing the evolution and explosion of their binary progenitors, *A&A* **624**, A66 (2019), arXiv:1804.09164 [astro-ph.SR].
- [140] D. D. Hendriks, L. A. C. van Son, M. Renzo, R. G. Izzard, and R. Farmer, Pulsational pair-instability supernovae in gravitational-wave and electromagnetic transients, *MNRAS* **526**, 4130 (2023), arXiv:2309.09339 [astro-ph.HE].

- [141] D. Chattopadhyay, J. Stegmann, F. Antonini, J. Barber, and I. M. Romero-Shaw, Double black hole mergers in nuclear star clusters: eccentricities, spins, masses, and the growth of massive seeds, *MNRAS* **526**, 4908 (2023), arXiv:2308.10884 [astro-ph.HE].
- [142] M. Fishbach, D. E. Holz, and B. Farr, Are LIGO's Black Holes Made from Smaller Black Holes?, *ApJL* **840**, L24 (2017), arXiv:1703.06869 [astro-ph.HE].
- [143] P. Mahapatra, A. Gupta, M. Favata, K. G. Arun, and B. S. Sathyaprakash, Remnant Black Hole Kicks and Implications for Hierarchical Mergers, *ApJL* **918**, L31 (2021), arXiv:2106.07179 [astro-ph.HE].
- [144] M. Zevin and D. E. Holz, Avoiding a Cluster Catastrophe: Retention Efficiency and the Binary Black Hole Mass Spectrum, arXiv e-prints, arXiv:2205.08549 (2022), arXiv:2205.08549 [astro-ph.HE].
- [145] H.-T. Janka, Natal kicks of stellar mass black holes by asymmetric mass ejection in fallback supernovae, *MNRAS* **434**, 1355 (2013).
- [146] C. Chan, B. Müller, and A. Heger, The impact of fallback on the compact remnants and chemical yields of core-collapse supernovae, *Monthly Notices of the Royal Astronomical Society* **495**, 3751–3762 (2020).
- [147] E. Gaburov, J. C. Lombardi, and S. Portegies Zwart, Mixing in massive stellar mergers, *MNRAS* **383**, L5 (2008), arXiv:0707.3021.
- [148] U. N. Di Carlo, M. Mapelli, M. Pasquato, S. Rastello, A. Ballone, M. Dall'Amico, N. Giacobbo, G. Iorio, M. Spera, S. Torniamenti, and F. Haardt, Intermediate-mass black holes from stellar mergers in young star clusters, *MNRAS* **507**, 5132 (2021), arXiv:2105.01085 [astro-ph.GA].
- [149] M. Dall'Amico, M. Mapelli, G. Iorio, G. Costa, S. Charlot, E. Korb, C. Sgalletta, and M. Lecroq, Impact of accretion-induced chemically homogeneous evolution on stellar and compact binary populations, *A&A* **695**, A221 (2025), arXiv:2501.04778 [astro-ph.HE].
- [150] J. Riley, I. Mandel, P. Marchant, E. Butler, K. Nathaniel, C. Neijssel, S. Shortt, and A. Vigna-Gómez, Chemically homogeneous evolution: a rapid population synthesis approach, *MNRAS* **505**, 663 (2021), arXiv:2010.00002 [astro-ph.SR].
- [151] I. Mandel and S. E. De Mink, Merging binary black holes formed through chemically homogeneous evolution in short-period stellar binaries, *MNRAS* **458**, 2634 (2016).
- [152] S. E. De Mink and I. Mandel, The chemically homogeneous evolutionary channel for binary black hole mergers: rates and properties of gravitational-wave events detectable by advanced LIGO, *MNRAS* **460**, 3545 (2016).
- [153] A. Ray and V. Kalogera, Reexamining Evidence of a Pair-Instability Mass Gap in the Binary Black Hole Population, arXiv e-prints, arXiv:2510.18867 (2025), arXiv:2510.18867 [astro-ph.HE].
- [154] D. Phan, N. Pradhan, and M. Jankowiak, Composable Effects for Flexible and Accelerated Probabilistic Programming in NumPyro, arXiv e-prints, arXiv:1912.11554 (2019), arXiv:1912.11554 [stat.ML].
- [155] J. Bradbury, R. Frostig, P. Hawkins, M. J. Johnson, C. Leary, D. Maclaurin, G. Necula, A. Paszke, J. VanderPlas, S. Wanderman-Milne, and Q. Zhang, JAX: composable transformations of Python+NumPy programs (2018).
- [156] F. Antonini, T. Callister, F. Dosopoulou, I. M. Romero-Shaw, and D. Chattopadhyay, Inferring the pair-instability mass gap from gravitational wave data, *Phys. Rev. D* **112**, 063040 (2025).
- [157] M. Fishbach, D. E. Holz, and W. M. Farr, Does the black hole merger rate evolve with redshift?, *The Astrophysical Journal Letters* **863**, L41 (2018).
- [158] R. Essick and W. Farr, Precision requirements for monte carlo sums within hierarchical bayesian inference (2022), arXiv:2204.00461 [astro-ph.IM].
- [159] The LIGO Scientific Collaboration, The Virgo Collaboration, and the KAGRA Collaboration, GWTC-4.0: Updating the Gravitational-Wave Transient Catalog with Observations from the First Part of the Fourth LIGO-Virgo-KAGRA Observing Run, arXiv e-prints, arXiv:2508.18082 (2025), arXiv:2508.18082 [gr-qc].

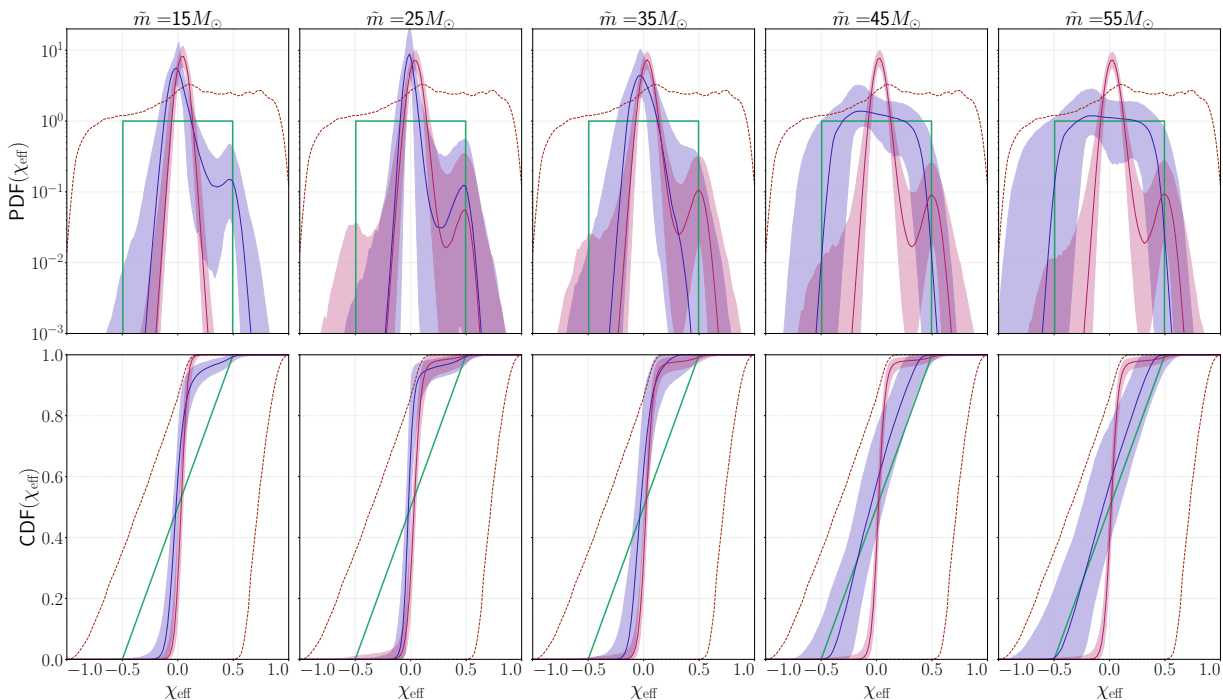


Figure S1. Inferred effective-spin distributions for different choices of the transition mass scale \tilde{m} . Columns correspond to $\tilde{m} = 15, 25, 35, 45,$ and $55 M_{\odot}$, respectively. The top panels show the inferred probability density functions, while the bottom panels show the corresponding cumulative distribution functions. Blue and pink curves indicate the two populations below and above \tilde{m} , respectively. Shaded regions denote the 90% credible intervals, and solid lines the median. The green curve shows the uniform distribution expected for hierarchical mergers in dense clusters [26]. The red dashed curves indicate the broad isotropic-spin priors used in the analysis.

Supplementary Material

ADDITIONAL SPIN POPULATION MODELS

Here we consider an additional set of population models in which the effective-spin distribution is a mixture of two independent Gaussian-process components separated by a transition mass scale \tilde{m} . The first component describes binaries with primary masses below \tilde{m} , while the second describes binaries above \tilde{m} . Rather than inferring \tilde{m} directly from the data, we fix its value and repeat the analysis for different choices of \tilde{m} . This approach complements the approach presented in the main text and allows us to probe how the inferred χ_{eff} distribution changes as progressively higher-mass binaries are included in the high-mass population, thereby identifying the mass scales at which transitions in the spin distribution occur. These results are consistent and reinforce the conclusions drawn in the main text.

Figure S1 shows the inferred effective-spin distributions for different choices of the transition mass scale \tilde{m} . The blue and red curves correspond to the low- and high-mass subpopulations, respectively. By varying \tilde{m} , we directly probe how the inferred χ_{eff} distribution changes with primary mass.

Below $15 M_{\odot}$, the effective-spin distribution is well described by a narrow approximately Normal distribution with a small positive mean and little evidence for extended tails. In this regime, the data do not require a broad isotropic-spin component. This behavior is broadly consistent with previous population analyses of the entire population, likely because the majority of observed BBH mergers are concentrated within the $10 M_{\odot}$ peak and therefore dominate population-averaged measurements.

Above $15 M_{\odot}$, however, the inferred χ_{eff} distribution changes significantly. The distribution becomes centered closer to $\chi_{\text{eff}} \simeq 0$ and develops broader support toward both positive and negative values, together with a possible excess of positive- $\chi_{\text{eff}} \simeq 0.5$ systems. The data confidently exclude models in which the low- and high-mass spin populations are statistically consistent with one another.

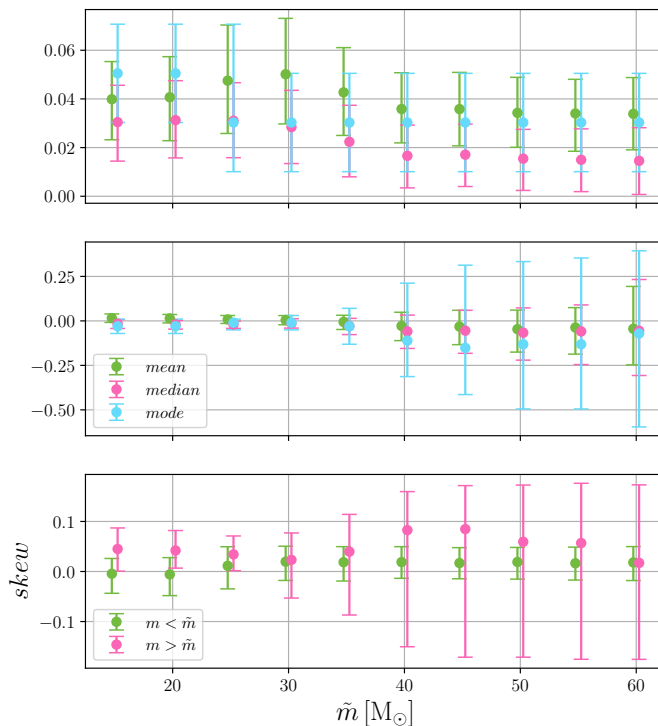


Figure S2. The evolution of the inferred effective-spin distributions as a function of the transition mass scale \tilde{m} . Error bars indicate the 90% credible intervals. The top panel shows the inferred mean, median and mode of the effective spin of the population with $m_1 < \tilde{m}$. The middle panel shows the inferred mean, median, and mode of the population with $m_1 > \tilde{m}$, illustrating the progressive shift of the high-mass population toward $\chi_{\text{eff}} \simeq 0$ and the increasing uncertainty associated with broader spin distributions at large masses. The bottom panel shows the Pearson first skewness coefficient, quantifying the degree of asymmetry of the inferred χ_{eff} distributions. While all measurements remain statistically consistent with symmetric distributions, the intermediate-mass regime exhibits tentative evidence for positive skewness associated with the possible excess near $\chi_{\text{eff}} \sim 0.5$.

For $\tilde{m} \gtrsim 20 M_\odot$, both the low- and high-mass populations develop a possible asymmetric tail with excess support near $\chi_{\text{eff}} \sim 0.5$, similar to features identified in recent concurrent studies [73, 105, 106, 153]. Since this excess disappears for $\tilde{m} \lesssim 15 M_\odot$ and for $\tilde{m} \gtrsim 30 M_\odot$, it appears to be associated primarily with systems in the mass range $15 \lesssim m_1/M_\odot \lesssim 30$, in agreement with our main analysis. Interestingly, $\chi_{\text{eff}} \sim 0.5$ is close to the value naturally expected from hierarchical mergers. When partially aligned with the orbital angular momentum, such systems can produce effective spins near the observed value.

For transition masses $\tilde{m} \gtrsim 45 M_\odot$, the inferred high-mass population becomes substantially broader and develops support extending over a large fraction of the allowed χ_{eff} range. The corresponding cumulative distributions flatten significantly, approaching the behavior expected for a broad isotropic-spin population associated with hierarchical mergers. By contrast, the low-mass population remains dominated by a narrow distribution centered near $\chi_{\text{eff}} \simeq 0.05$, with evidence for a broader possibly asymmetric component. The inferred high-mass spin distributions therefore become qualitatively consistent with the isotropic-spin population inferred in our previous work [22, 26].

Figure S2 provides a compact summary of how the inferred effective-spin distributions evolve as the transition mass scale \tilde{m} is varied. The mean, median, and mode of the low mass population remain consistently positive and peaked around $\chi_{\text{eff}} \simeq 0.03$, while the inferred skewness with respect to its mode stays consistent with zero. This behavior reflects the fact that the majority of BBH mergers are concentrated within the $10 M_\odot$ peak, which therefore dominates the inferred low-mass distribution whenever included in the analysis.

By contrast, the properties of the high-mass population evolve significantly as \tilde{m} increases. For $\tilde{m} \lesssim 30 M_\odot$, the high-mass population retains a small positive shift in χ_{eff} , but above this scale the distribution progressively moves toward $\chi_{\text{eff}} \simeq 0$ and becomes substantially broader. The increasing uncertainties in the mode and skewness reflect the emergence of broad spin distributions with extended support toward both positive and negative effective spins. While the inferred skewness remains statistically consistent with zero at all masses, the data show tentative evidence for a positive tail in the intermediate-mass regime, consistent with the possible excess towards $\chi_{\text{eff}} \sim 0.5$ identified in the full posterior distributions. However, as discussed in the main text, this apparent excess may instead reflect the

difficulty of accurately modeling selection effects that preferentially favor positive χ_{eff} in sparsely populated regions of parameter space.

HIERARCHICAL INFERENCE AND DATA

We perform hierarchical population inference using a Hamiltonian Monte Carlo (HMC) method, implemented in `numpyro` [154] using `jax` [155], following the procedure laid out in [156]. We begin by defining the posterior probabilities for hyperparameters Λ , given a set of observed data $\{d_i\}$

$$p(\Lambda|\{d_i\}) \propto p(\Lambda) \xi^{-N_{\text{det}}}(\Lambda) \prod_{i=1}^{N_{\text{det}}} \left\langle \frac{p(\theta_i | \lambda)}{p_{\text{pe}}(\theta_i)} \right\rangle. \quad (\text{S1})$$

Where $p(\Lambda)$ are the population parameter priors and $p_{\text{pe}}(\theta_i)$ is the single-event parameter estimation prior. We take an average over the posterior samples for each event i [156, 157]. Selection effects are accounted for using the detection efficiency;

$$\xi(\Lambda) = \frac{1}{N_{\text{inj}}} \sum_{i=1}^{N_{\text{found}}} \frac{p(\theta_i|\Lambda)}{p_{\text{inj}}(\theta_i)}. \quad (\text{S2})$$

This re-weights the recovered injections from a reference injection distribution $p_{\text{inj}}(\theta_i)$, giving the total fraction of events expected to pass our detection criteria.

We track the number of effective posterior samples N_{eff} for each event to control Monte Carlo noise while sampling

$$N_{\text{eff}}(\Lambda) = \frac{\left[\sum_j w_{i,j}(\Lambda) \right]^2}{\sum_j w_{i,j}^2(\Lambda)}, \quad w_{i,j} = \frac{p(\theta_{i,j}|\Lambda)}{p_{\text{pe}}(\theta_{i,j})}, \quad (\text{S3})$$

and similarly for the injections we track,

$$N_{\text{eff}}^{\text{inj}}(\Lambda) = \frac{\left[\sum_i w_i(\Lambda) \right]^2}{\sum_i w_i^2(\Lambda)}. \quad (\text{S4})$$

Following [158], we require $N_{\text{eff}}^{\text{inj}}(\Lambda) \gtrsim 4N_{\text{det}}$. As opposed to hard-cuts, we add penalties to the log-likelihood to exclude poorly sampled regions of the parameter space,

$$\ln S \left(\frac{N_{\text{eff}}^{\text{inj}}(\Lambda)}{4N_{\text{det}}} \right) + \ln S \left(\frac{\mathcal{N}}{0.6} \right), \quad S(x) = \frac{1}{1+x^{-30}}, \quad \mathcal{N} \equiv \min_i \log N_{\text{eff},i}. \quad (\text{S5})$$

This allows for the inference to smoothly suppress models where either the injection set or the events are represented by too few effective samples.

For events from GWTC-1 [3], we use the parameter estimation samples *Overall posterior*. For sources found in GWTC-2 [94], we use the parameter estimation samples *PrecessingSpinIMRHM*, and for events found in GWTC-3 [91], we use *C01: Mixed* samples. For GWTC-4 [159] and GWTC-5 [6] events, we preferentially use *NRSur7dq4*. In the case of those samples being unavailable, we use *Mixed* samples for GWTC-4 and *IMRPhenomXPHM-SpinTaylor* samples for GWTC-5.

The prior choice for the hyper-parameters of our models are reported in Table S1. Figure S3 shows the recovered posteriors of key hyper-parameters for our models with $(\tilde{m}_{\text{low}}, \tilde{m}_{\text{high}}) = (50, 200)M_{\odot}$.

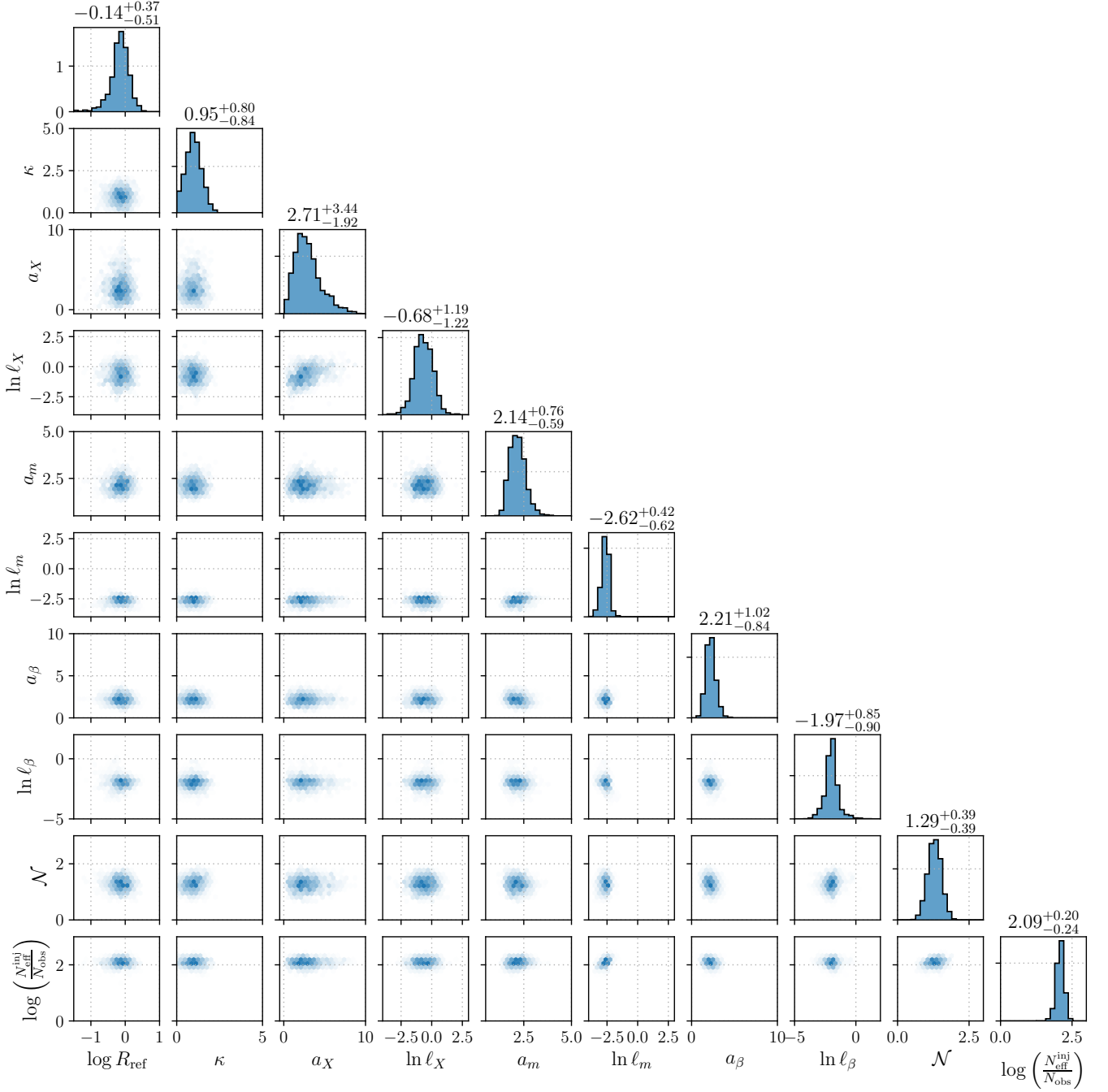


Figure S3. Posterior distributions of hyper-parameters for the mass-interval population models of Section II. Here, $N_{\text{inj}}^{\text{eff}}/N_{\text{obs}}$ gives the total number of injections divided by the number of detections. The quantity R_{ref} represents the differential merger-rate density, in units of $\text{Gpc}^{-3} \text{yr}^{-1} M_{\odot}^{-1}$, evaluated at $m_1 = 20 M_{\odot}$ and redshift $z = 0.2$. In this model we set $(\tilde{m}_{\text{low}}, \tilde{m}_{\text{high}}) = (18, 30) M_{\odot}$.

Parameter	Prior	Defined in
a_{m_1}	$\mathcal{HN}(0.8)$	m_1 Model
$\ln l_{m_1}$	$\mathcal{N}(-0.2, 1)$	m_1 Model
a_{β_q}	$\mathcal{HN}(1.0)$	β_q Model
$\ln l_{\beta_q}$	$\mathcal{N}(-0.5, 1)$	β_q Model
$a_{\chi_{eff}}$	$\mathcal{HN}(3)$	χ_{eff} Model
$\ln l_{\chi_{eff}}$	$\mathcal{N}(-0.5, 0.9)$	χ_{eff} Model
χ_{\max}	$\mathcal{U}[0.05, 1]$	χ_{eff} Model
$\chi_{\min, \text{unscaled}}$	$\mathcal{U}[0, 1]$	χ_{eff} Model
μ	$\mathcal{U}(-1)$	$p_{\text{out}}(\chi_{\text{eff}} m_1)$ Model
σ	$\mathcal{U}(-1.5, 0)$	$p_{\text{out}}(\chi_{\text{eff}} m_1)$ Model
$\chi_{\max, \text{out}}$	$\mathcal{U}[0.1, 1]$	$p_{\text{out}}(\chi_{\text{eff}} m_1)$ Model
$\chi_{\min, \text{unscaled, out}}$	$\mathcal{U}[0, 1]$	$p_{\text{out}}(\chi_{\text{eff}} m_1)$ Model
κ	$\mathcal{N}(0, 5)$	redshift Model

Table S1. Prior distributions for hyper-parameters of $p(\chi_{eff})$ and mass models used in the main text.